Steam Explosion Experiments at Intermediate Scale: FITSB Series

D. E. Mitchell, N. A. Evans

Prepared for
U. S. NUCLEAR REGULATORY COMMISSION

SF2900Q(8-81)

NOTICE

This report was prepared as an account of work sponsored by an agency of the United States Government. Neither the United States Government nor any agency thereof, or any of their employees, makes any warranty, expressed or implied, or assumes any legal liability or responsibility for any third party's use, or the results of such use, of any information, apparatus product or process disclosed in this report, or represents that its use by such third party would not infringe privately owned rights.

STEAM EXPLOSION EXPERIMENTS AT
INTERMEDIATE SCALE: FITSB SERIES

D. E. Mitchell
N. A. Evans

ABSTRACT

Experiments in the FITS chamber have been performed in which 18.7 kg of molten iron-alumina core melt simulant was delivered into water chambers in which the water mass was 1.5 to 15 times greater than the melt. Experiments in subcooled water showed that spontaneous explosions occurred over the range of water/melt mass ratio and geometry used and that in certain experiments, double explosions occurred. With double explosions, the first explosion enhanced fuel-coolant mixing for the second explosion. In one test in saturated water, multiple trigger sites were observed but no propagating explosion resulted. Two distinct, but additive, energy conversion ratios were calculated from the test results. Based on pressure records and debris velocities, a kinetic energy conversion ratio, η_{KE}, had calculated values between 0.3 and 1.6 percent. A conversion ratio, η_D, related to the work done in pressurizing the chamber air ranged between 0.2 percent and 8.6 percent. The total fraction of the melt thermal energy converted, $\eta_{tot} = \eta_{KE} + \eta_D$, reached a value of 9.9 percent in an experiment involving a double explosion, but in this case, the value of η_{KE} was limited to 1.3 percent.

CONTENTS

LIST OF FIGURES

LIST OF TABLES

STEAM EXPLOSION EXPERIMENTS AT
INTERMEDIATE SCALE: FITSB SERIES

1. INTRODUCTION

During the past several years, work has been under way at this laboratory to determine the damage potential of steam explosions that might result from molten core-coolant interactions. By steam explosion, we mean the explosive boiling of the coolant when it comes in contact and mixes with molten fuel in reactions that are observed to propagate through the fuel-coolant mixture at rates of 200 to 600 m/s. These explosions are characterized by short (order of a 100 µs) pressure rise times and postreaction debris that are of the order of 220 µm mass average diameter.

Numerous investigators have studied the energetics of these interactions and have used various simulants ranging from molten salt at approximately 1200 K[1] to thermite-generated melts consisting of metal-metal oxide compositions at temperatures up to 2700 K.[2-4] Masses ranged from tens of milligrams to a few kilograms. Some of these studies have included the effects of parameters such as water subcooling, system pressure, and contact mode.[5] All of the above experimental methods have been able to produce values for conversion ratio, defined as the ratio of work or kinetic energy produced to the initial melt thermal energy. These conversion ratios ranged between 0.05 percent and 3 percent, depending on the initial and boundary conditions of the experiment and the method used for estimating the amount of fuel that participated.

Since quantities of fuel that are available to participate in a steam explosion can be of the order of many metric tons in a Light Water Reactor (LWR) and most of the experiments are done with much smaller quantities, it is not clear if the results from these small and intermediate scale experiments can be extrapolated to reactor scale. We have attempted to address the scaling issue by developing experimental methods and performing analyses that can better quantify the initial conditions leading to a steam explosion, and to provide data that can be used to construct mathematical[6] models of the processes that would aid in extending the results to reactor scale.[7]

Most of our experimental results to date have used molten iron-alumina, which has been shown to be a good fuel simulant when compared with results (such as mixing, propagation, and conversion ratio) from tests using corium A+R consisting of UO_2, ZrO_2, and stainless steel.[8]

The work described in this paper is an extension of the work reported in Reference 9, where 2 to 5 kg of molten iron-alumina simulants were dropped into cubical chambers containing subcooled water at initial water-to-fuel mass ratios nominally 40:1. Those experiments showed that the steam explosion process could be divided into five distinct areas (melt entry, mixing, triggering, propagation, and expansion) and that about 1 percent to 3 percent of the thermal energy in the initial melt mass was converted to kinetic energy of the debris. The current experiments were done using 18.7 kg of iron-alumina simulant delivered into water chambers that resulted in initial water/melt mass ratios from 1.5:1 to 15:1. We have observed differences in behavior in these experiments (where the melt masses are larger and the water/melt mass ratio is smaller) compared to the experiments described in Reference 9. This paper describes the differences that are attributed to the increased melt mass, the variation of mass ratio, and the change in water chamber dimensions.

2. EXPERIMENTAL APPARATUS AND PROCEDURE

The experiments were conducted in the FITS chamber shown in Figure 1 and described in detail in Reference 9. Improvements in instrumentation, melt delivery, and experiment control were incorporated, based on experience gained from earlier work. The improvements consisted of improved experiment control; a redesigned melt delivery system (including melt retention and crucible modifications); and instrumentation to measure thermite burn rate, FITS chamber gas phase temperature and pressure, debris slug velocity, and water phase pressure, together with debris characterization methods. Appendix A describes the new melt injection sequence control that represents the most significant improvement in the experimental method. Water chambers used for these experiments were identical to those described in References 9 and 10; the contained water volumes were rectangular in shape with square, open surfaces. The water chambers were fabricated from 6.3-mm thick plexiglass stock in sizes calculated to result in initial water to melt mass ratios of 1.5:1 to 15:1. Figure 2 shows the configuration of a typical water chamber and associated instrumentation.

The experiments were instrumented with pressure transducers: in the water chamber base and side walls to measure water phase pressure; in the FITS chamber upper head to study debris slug characteristics; and in the FITS chamber side wall ports to measure the gas phase pressure. Melt delivery was initiated automatically through the use of probes in the crucible that sensed when the thermite reaction was complete. Melt entry time was measured by photodiodes 2.5 cm above the water surface; shape and velocity of the melt at water impact and during mixing were recorded by high speed cameras. Debris recovered from the experiments was characterized by sieving using sieve sizes ranging from 38 μm to 25 mm.

The fuel used in these experiments was prepared by a metallothermic reaction. The initial reactants were magnetite (Fe_3O_4, -200/30 mesh) and pure aluminum (99.7 percent, -325/75 mesh) in the ratio of 76.3 w/% Fe_3O_4 and 23.7 w/% Al. The reaction is given by

$$3Fe_3O_4 + 8Al \rightarrow 9Fe + 4Al_2O_3 + 795 \text{ kcal} \quad .$$

The resulting melt consisted of 55 w/% Fe and 45 w/% Al_2O_3 at a theoretical (maximum) temperature of 3100 K and an energy content of 3.3 MJ/kg.

One experiment was done to determine the thermal energy content of the melt. In this experiment, 1.46 kg of melt was

Melt Transport

Graphite Crucible and Charge

Igniter and Melt Observ.

Thermite Burn Rate monitor and Delivery Control

0

5.7 cm Melt Release

Debris Slug Impact Conditions (Pressure and Arrival Time)

Hi-Cam 4000 ips

Removable Head

Access Walk

Debris Deflector

Burst Diaphragm (Over Pressure Protection)

Gas Phase Pressure and Temperature

Main Containment 2.4 MPa w.p 5.6 M^3 Volume

Water Phase Pressure

Water Level

Hi-Cam 8000 fps

151-279 cm

Instrument Feed-Thru Ports

Hi-Cam 8000 fps

Lucite Chamber

Gas Phase Pressure and Temperature

Water Chamber Base Pressure Gage Mounting

Water Chamber Support
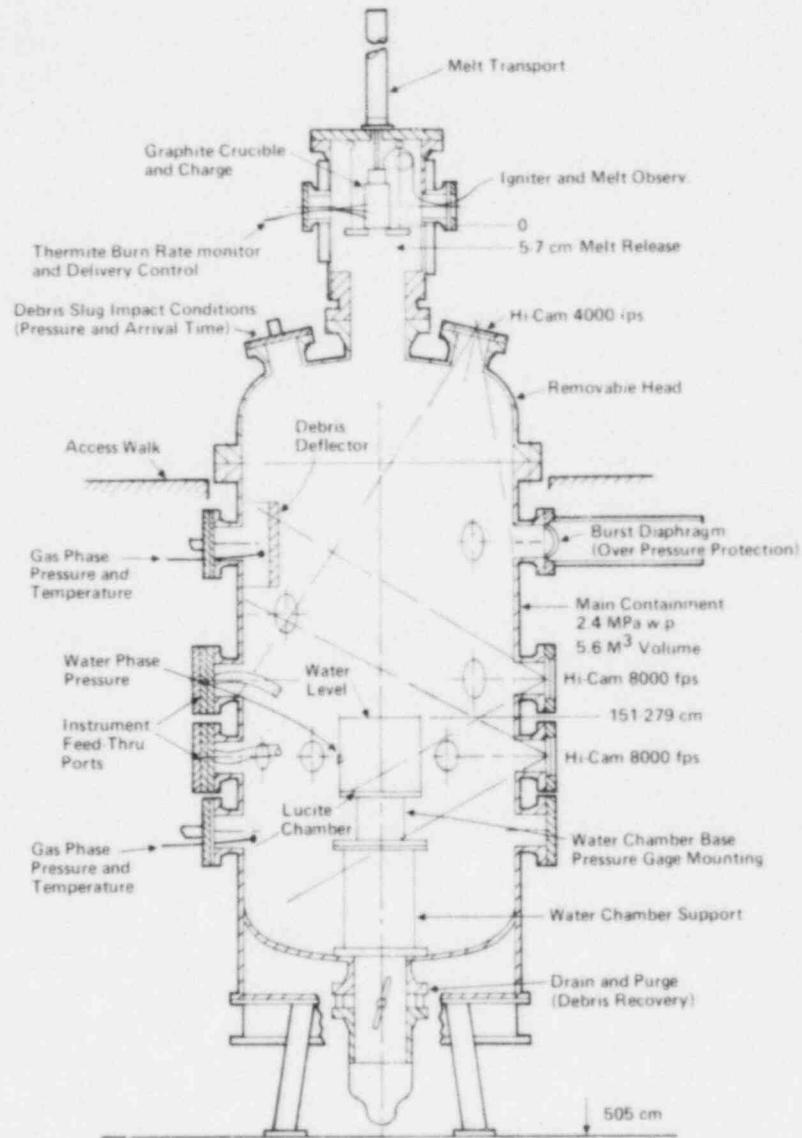
Drain and Purge (Debris Recovery)
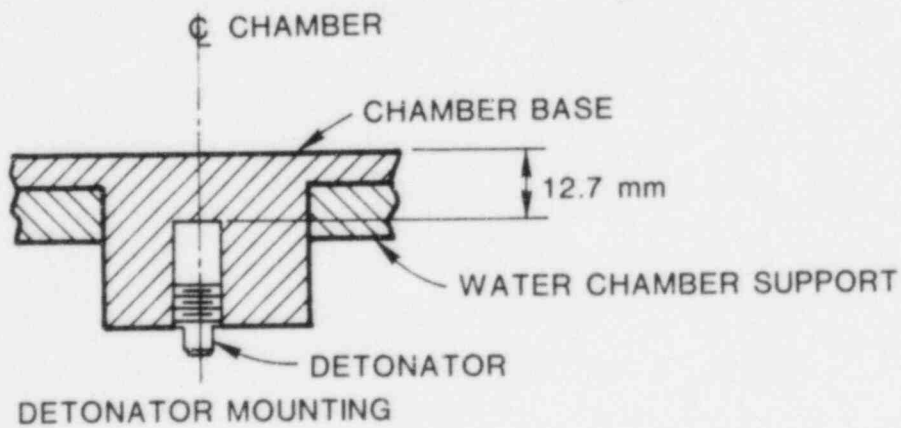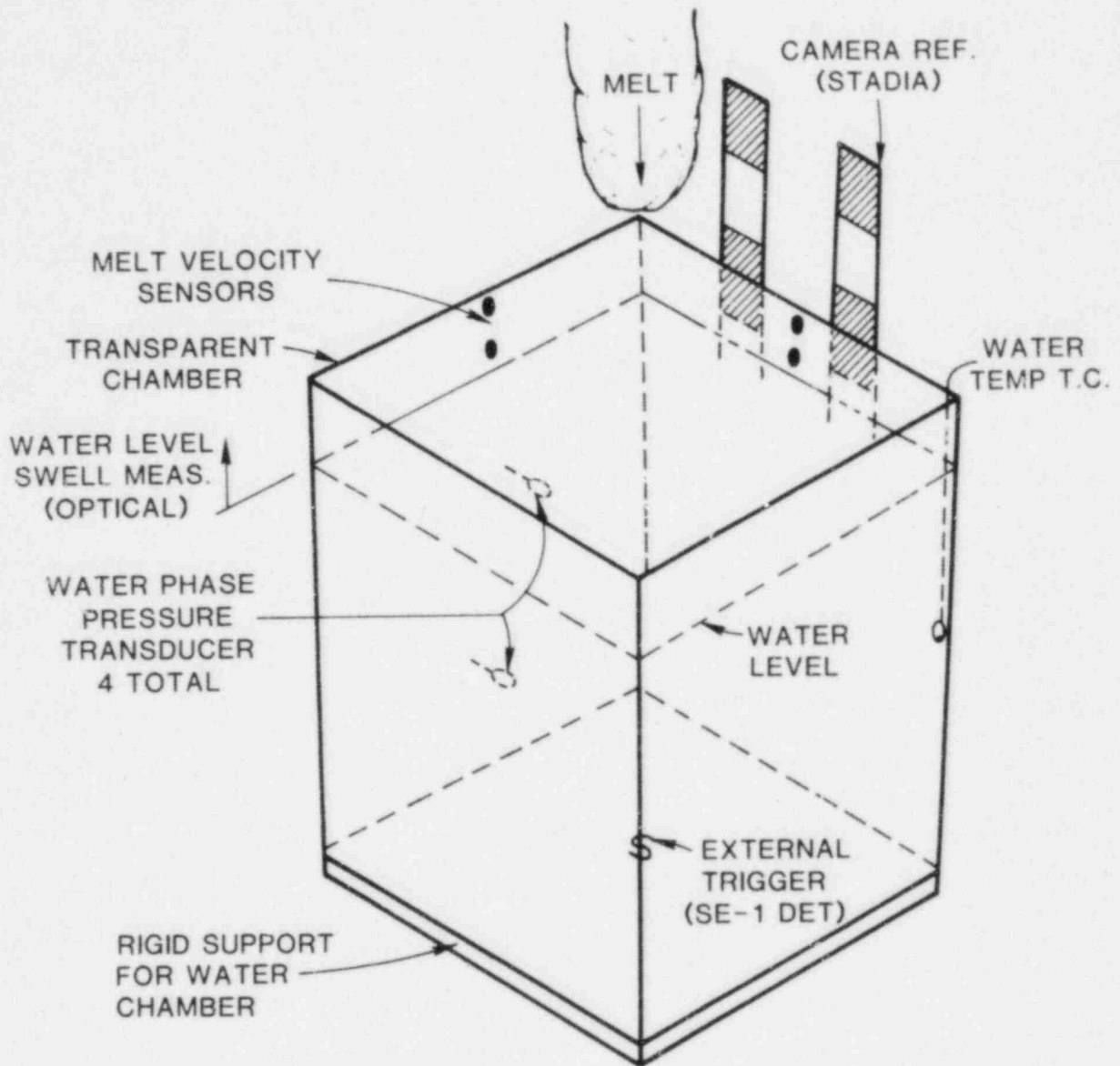
505 cm

Figure 1. FITS Containment Chamber

Figure 2.   Typical Instrumented Water Chamber

delivered into 41.6 kg of water at 284 K. Based on the temperature rise of 24 K and a constant specific heat of water (4.19 J/g K) a value of 2.8 MJ/kg was calculated and is the value we have used consistently in reporting the conversion ratios in this report and in References 9 and 10.

Melt temperature at water entry was measured in one experiment to be 2750 K using a calibrated high-speed camera. The technique is useful for estimating the black body temperature at the surface of the melt mass, but the method does not supply any information related to the emissivity of the melt, and hence, the temperature calculated is a minimum; the melt temperature will increase for an actual emissivity less than unity.

The thermite was ignited using a 1.3-m length of No. 16 gauge nichrome wire wound in a spiral and located at the top surface of the initially mixed powder. A current of approximately 150 A (208 V) for 1.5 s was used to guarantee ignition. This method was safe and reliable and allowed the mixture to be ignited over the entire surface (410 cm^2) with reduced variability in the burn rate and provided improved experiment control in terms of active signals sensed for releasing the melt.

Water from the local water supply was used as the coolant. No special treatment, such as degassing or deionizing, was done. Water temperature was not controlled for the majority of the experiments and was between 309 and 319 K. Two experiments were done with saturated water at 368 K.

3. RESULTS AND DISCUSSION

3.1 Triggering and Propagation

In References 9 and 10, we described the steam explosion process and divided it into five separate phases: melt entry, mixing, triggering, propagation and expansion. The recent FITSB experiments showed that these phases were still distinct but that triggering and propagation are more complicated than was first reported in Reference 9.

As opposed to the more common base triggering phenomena observed in those experiments that used 2 to 5 kg of melt, we observed triggers that occurred randomly: at or near the water surface; at or near the water chamber base or side walls; on occasion, at all these locations. Some of these triggers escalated into a propagating wave through the melt-water mixture, while the remainder decayed locally with no continuing observable effect. When recorded by the cameras, triggers appeared as rather complicated wave-like phenomena in the water surrounding the melt-water mixture. Propagation of these waves had a similar appearance but occurred in the melt-water mixture and resulted in significant extinction of melt luminosity. In addition to the differences in triggering, we also observed multiple explosion events. Three of the experiments (FITS1B, 4B, and 8B), having mass ratios of 12, 12, and 15, and water depths of 61, 61, and 76.5 cm, respectively, resulted in double explosions; i.e., there were two explosive interactions in each experiment.

The FITS experiments were instrumented with pressure transducers in the water chamber, FITS chamber upper head, and FITS chamber side walls. Temperatures were measured in the water chamber and in conjunction with FITS chamber wall pressures. The data presented here are those obtained from the FITS chamber air pressure and temperature transducers. The pressure transducers were located so that they responded to chamber gas phase pressure only and were not affected by debris. Thermocouples were exposed to the debris (water, melt, steam) and their response was more erratic.

A typical pressure record is shown schematically in Figure 3. The data are characterized by three distinct features (four in the case of a double explosion):

1. Air shock, present if the event is sufficient to rapidly pressurize the chamber air. There can be two of these, depending on the type of event.

2. Chamber equilibration, following the sudden chamber pressurization. The chamber gases equilibrated in approximately 20 ms resulting in a discernable pressure plateau that was indicative of the state

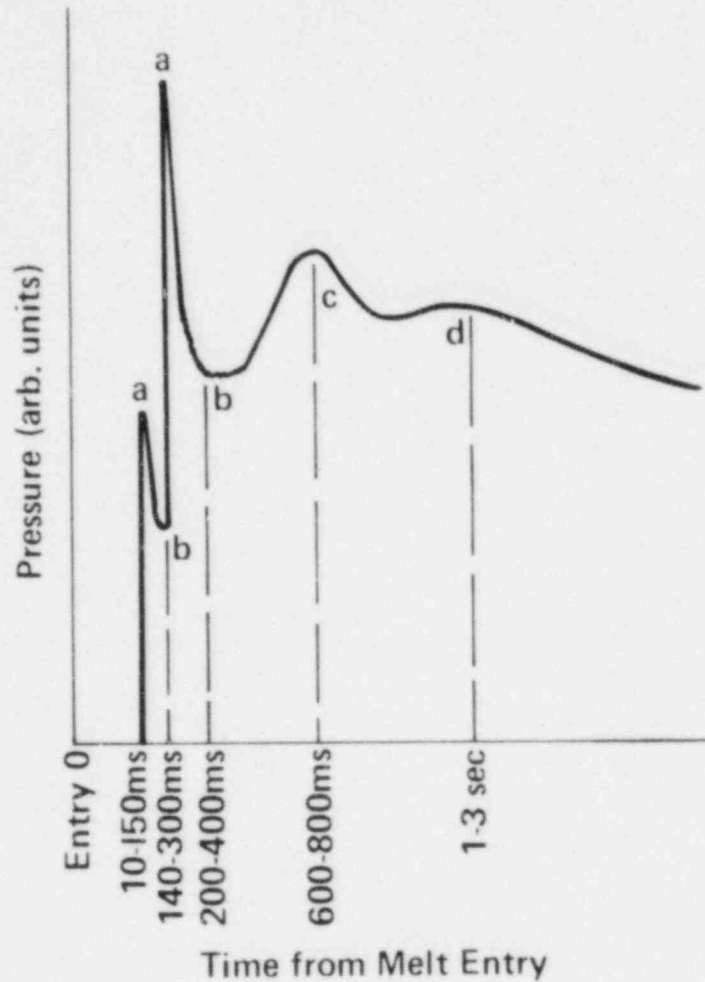Figure 3.   Schematic of a Typical FITSB Chamber Air Pressure History

a.   Pressurization Due to Steam Explosion(s). Two Peaks Present in Double Explosions.

b.   Quasi-static pressure plateau used for conversion ratio estimates.

c.   Late-time steam or hydrogen generation. Peak and rise time depend on the type of event (single or double explosion).

d.   Pressure Due to Debris Cooling in Chamber Base.

achieved in the chamber following the explosion and release of melt energy.

3. Chamber repressurization due to either hydrogen production and combustion and/or late-time steam generation due to residual molten debris cooling in the remaining water.

The peak pressure seen in the third event was lower for double explosion events than for a single event. This may have been due to the fact that more melt was involved in the double steam explosion and was not available for contributing to the steam or hydrogen production events.

3.2 Single Explosions

Table 1 describes the nine experiments conducted in the FITSB series, and a description of some of the important features is included below.

Experiments 2B, 3B, 7B, and 9B all resulted in single explosions triggered either at the water surface or water chamber base. The sequence of events leading to these explosions was similar to the earlier 2- to 5-kg experiments. Immediately after contact with the water, the melt was observed to fragment into droplets estimated to be between 10 and 20 mm in diameter. The fragmentation and mixing continued until the time of explosion trigger. Chamber air pressure records for these single explosions showed three characteristic features that depended on initial conditions such as water depth and mass ratio. These characteristics were a short rise time to the pressure peak; a relaxation in approximately 20 ms to a quasi-static plateau; and late-time chamber repressurization due to steam generation with possible augmentation by hydrogen production. Figures 4 through 7 are chamber air pressure records for these single-explosion events.

Figure 6 for FITS7B, at a mass ratio of 1.5:1, shows essentially no steam explosion peak, but a large steam generation pressure rise followed by what might have been a hydrogen combustion event. By contrast, Figure 7 for FITS9B, at a mass ratio of 9:1, shows a significant steam explosion pressure peak and associated pressure plateau followed by a modest steam generation pressure rise.

3.3 Double Explosions

Three of the experiments (FITS1B, 4B, and 8B, see Table 1), having mass ratios of 12, 12, and 15, and water depths of 61, 61, and 76.5 cm, respectively, resulted in double explosions; i.e. there were two explosive interactions separated by approximately 120 to 140 ms in each experiment. Chamber air pressure records for these double explosion events are

Table 1

FITSB Initial Conditions and Observations

Expt.	Melt Mass (kg)	Entry Vel. (m/s)	Avg. dia at Entry[a] (cm)	Water Geometry (cm) sq x deep	Water Mass (kg)	Water Temp (K)	Initial Ratio Water/Melt Mass	Initial Ratio Water/Melt Vol.[b]	Spontaneous Explosion Location	Spontaneous Explosion Time after Melt Entry (ms)	Other Observations
1B	18.7	5.4	4.1	61 x 61	226.0	298	12.0	46.0	Surface Unknown	142 275	First explosion Second explosion
2B	18.6	6.0	6.0	61 x 30	113.0	298	6.0	23.0	Surface	84	Single explosion
3B	18.6	6.0	24.0	43 x 30	57.0	295	3.0	11.5	Base	77	Single explosion weak interaction at surface at 70 ms after entry that did not propagate
4B	18.7	6.8	5.8	61 x 61	226.0	299	12.0	46.0	Surface Base	29 146	First explosion Second explosion
6B	18.7	7.2	6.5	46 x 30	63.4	367	3.4	12.9	none	---	Multiple interactions at 40, 57, 82 and 153 ms after melt entry, no propagation or steam explosion
7B	18.7	7.4	n.o.[c]	43 x 15.2	28.1	291	1.5	5.7	n.o.	80	No camera data, time estimated from water phase gauges
8B	18.7	6.5	29.0	61 x 76.5	283.5	288	15.0	57.4	Surface Base	27 146	First explosion Second explosion
9B	18.7	7.0	5.6	61 x 45.7	170.0	289	9.0	34.6	Base	98	Single explosion

[a] Optical measurement

[b] Melt density 3.8 g/cm^3

[c] Not observed

Figure 4a.   FITS2B Chamber Air Pressure

Figure 4b. FITS2B Chamber Air Pressure (expanded time scale)
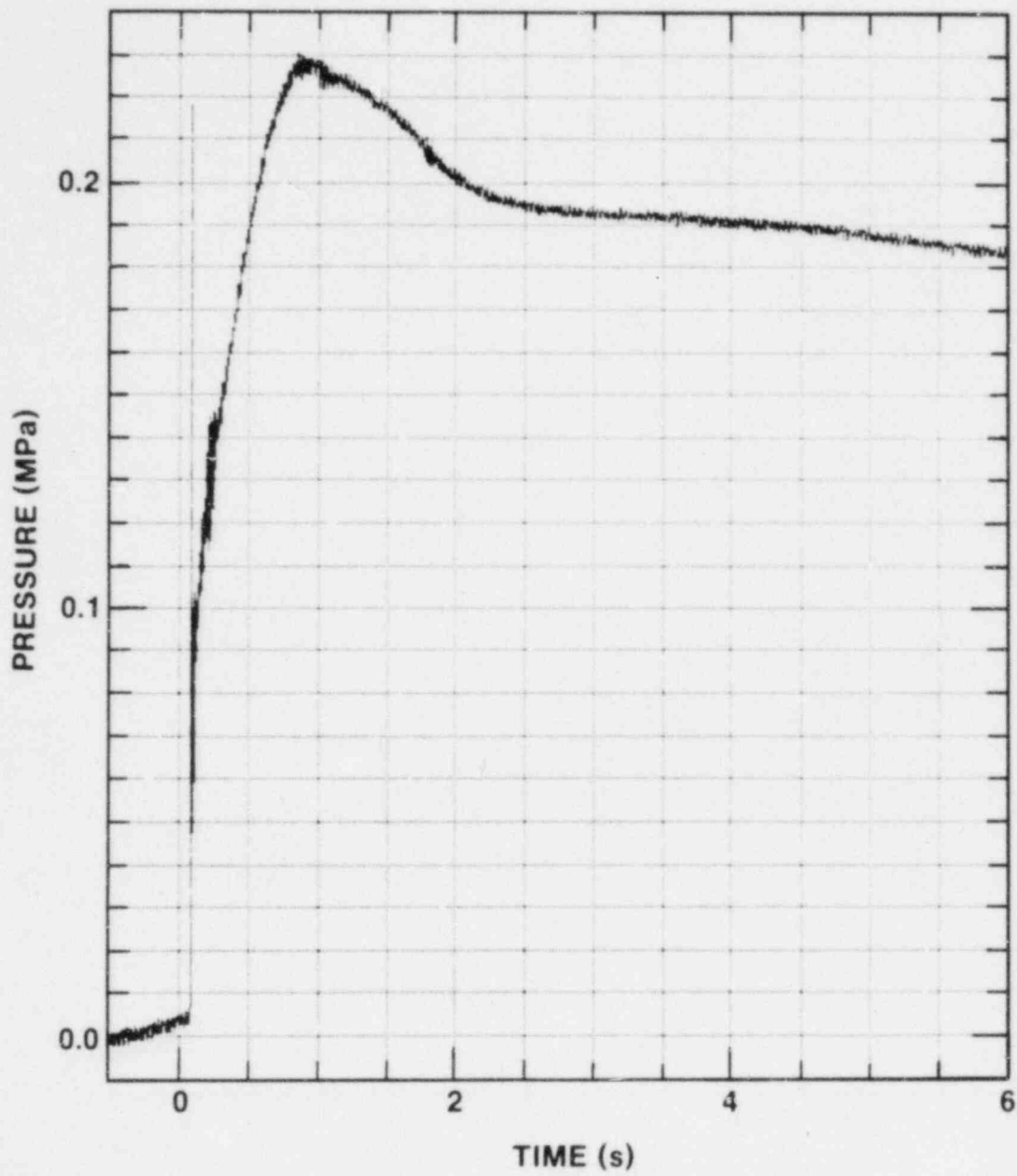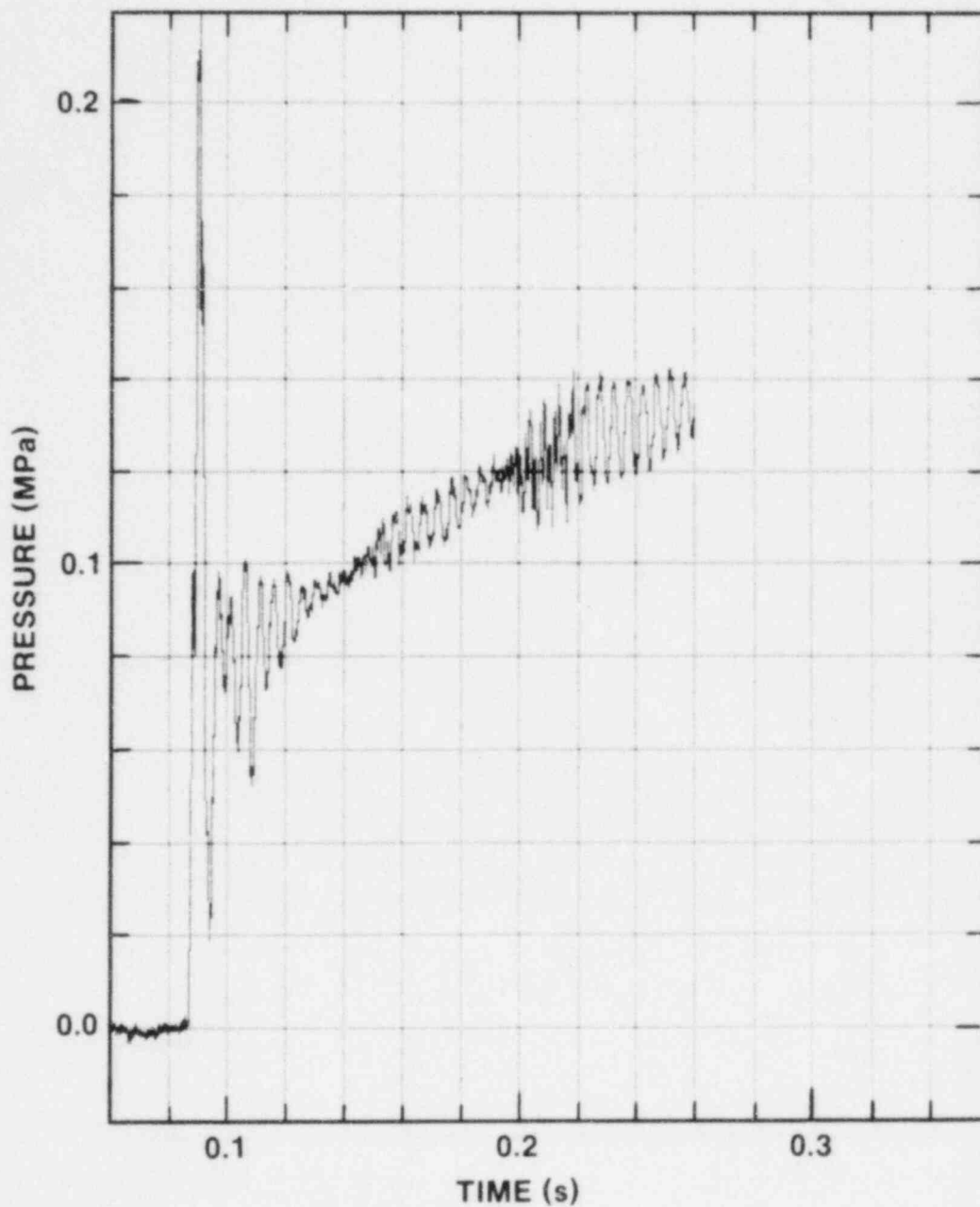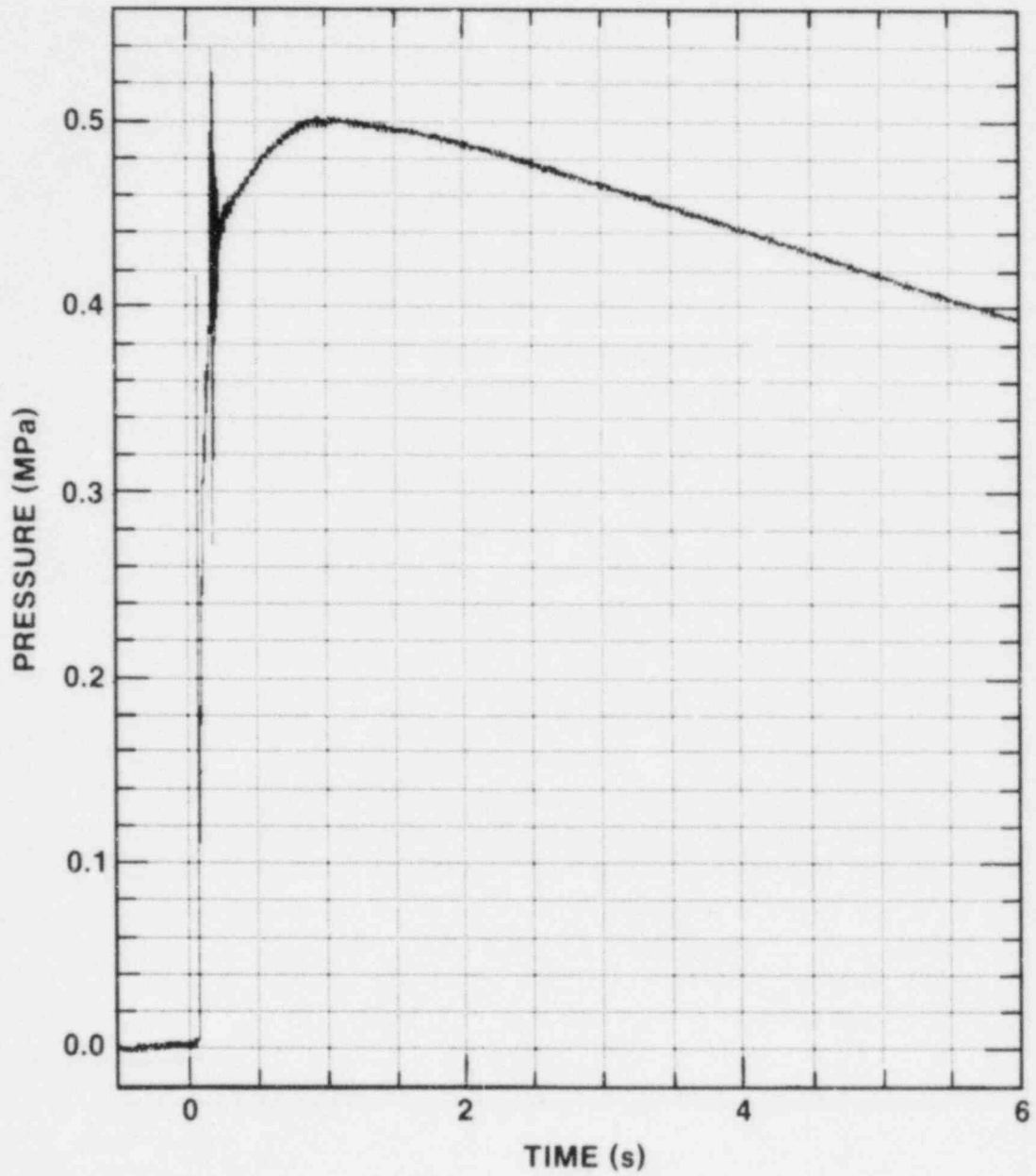
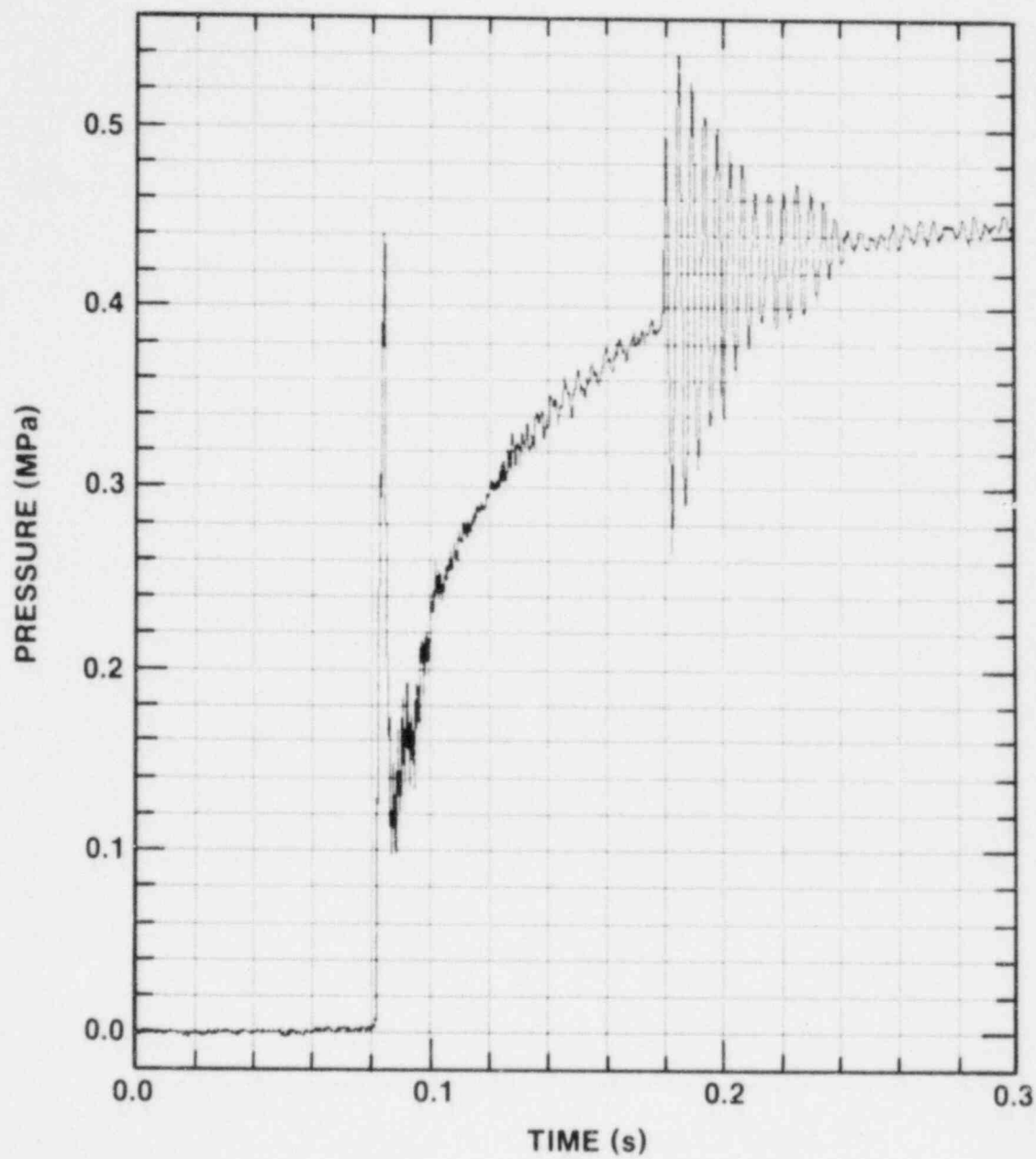Figure 5a. FITS3B Chamber Air Pressure

-13-

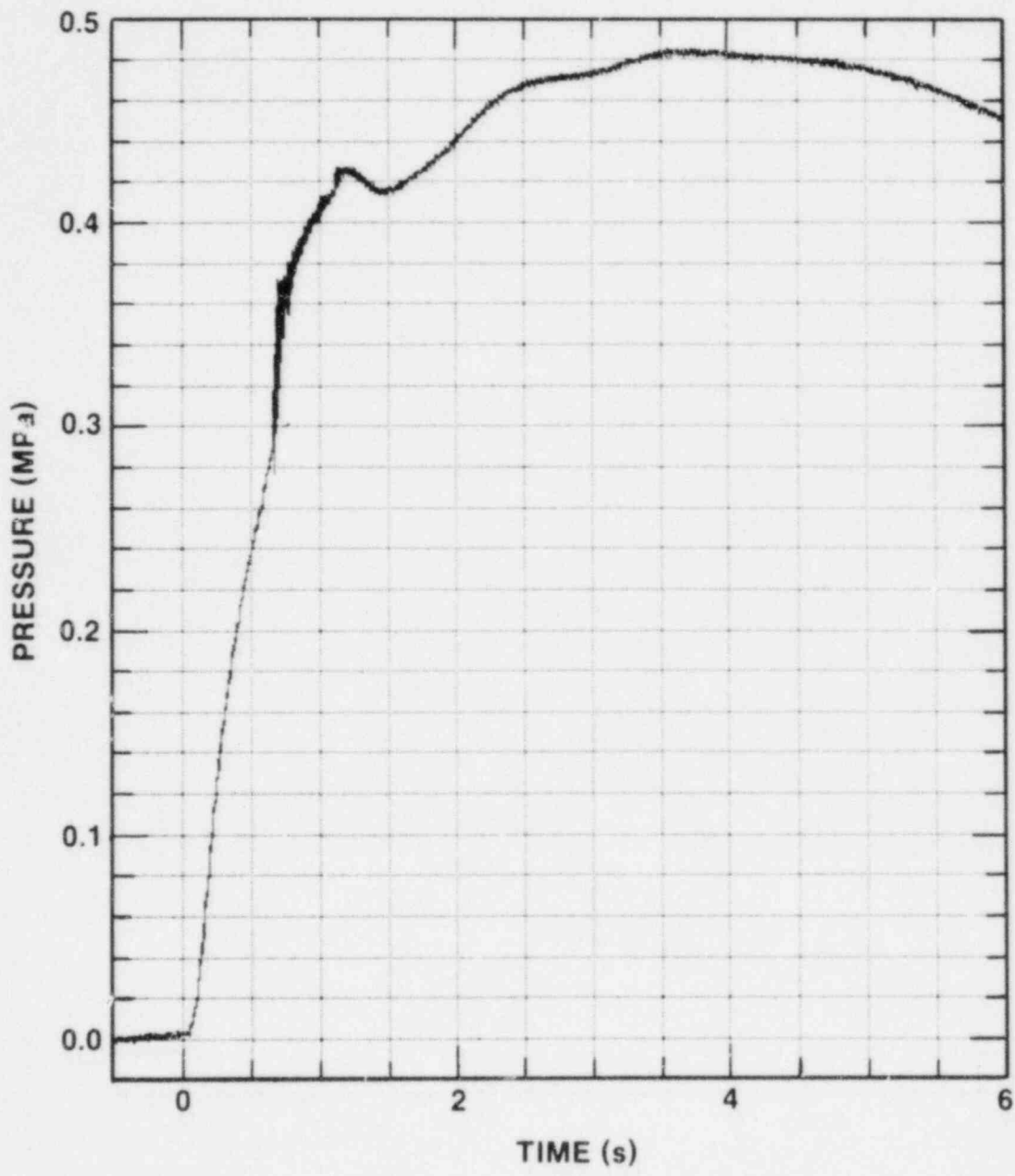Figure 5b. FITS3B Chamber Air Pressure (expanded time scale)

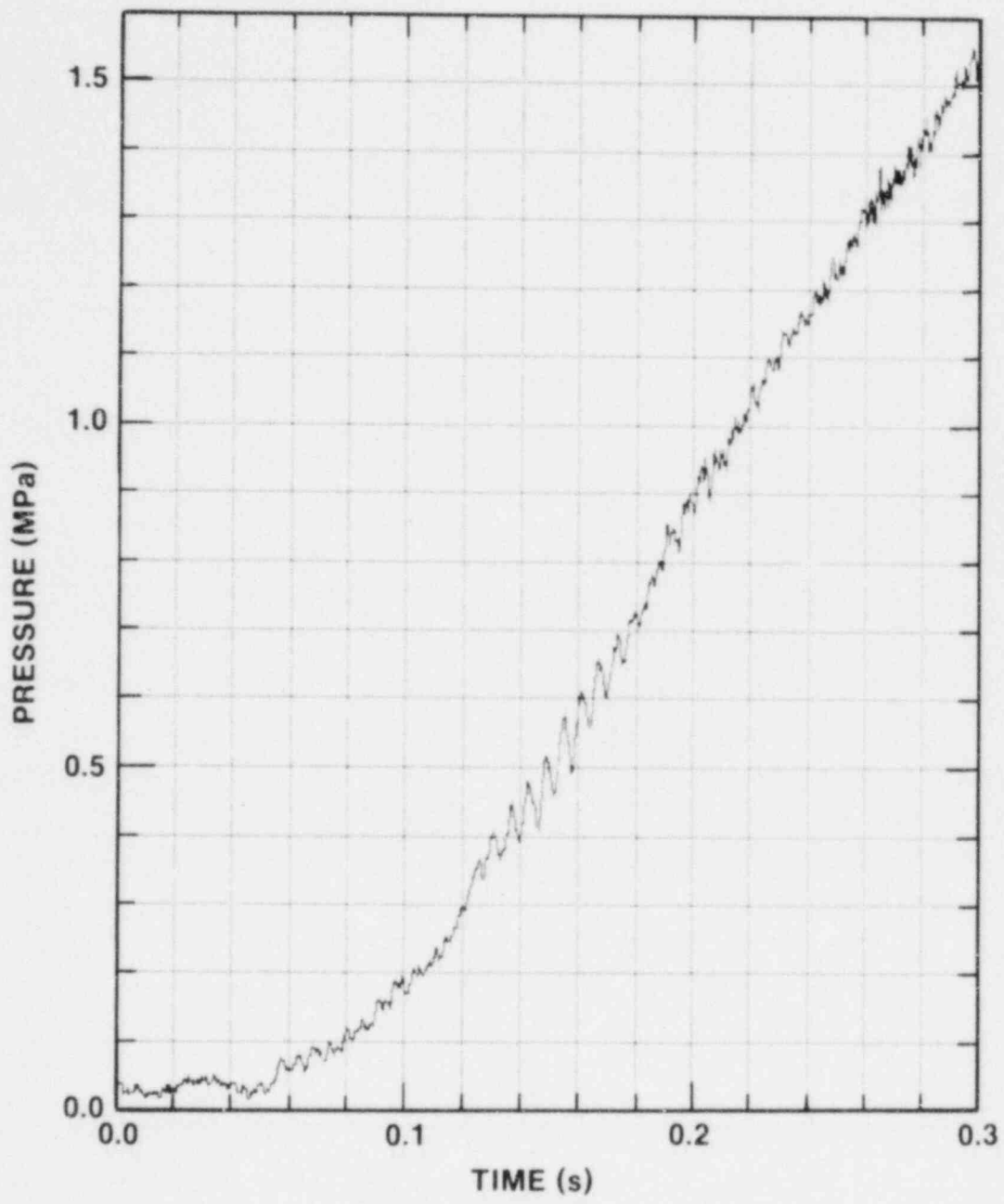Figure 6a. FITS7B Chamber Air Pressure (no camera data)

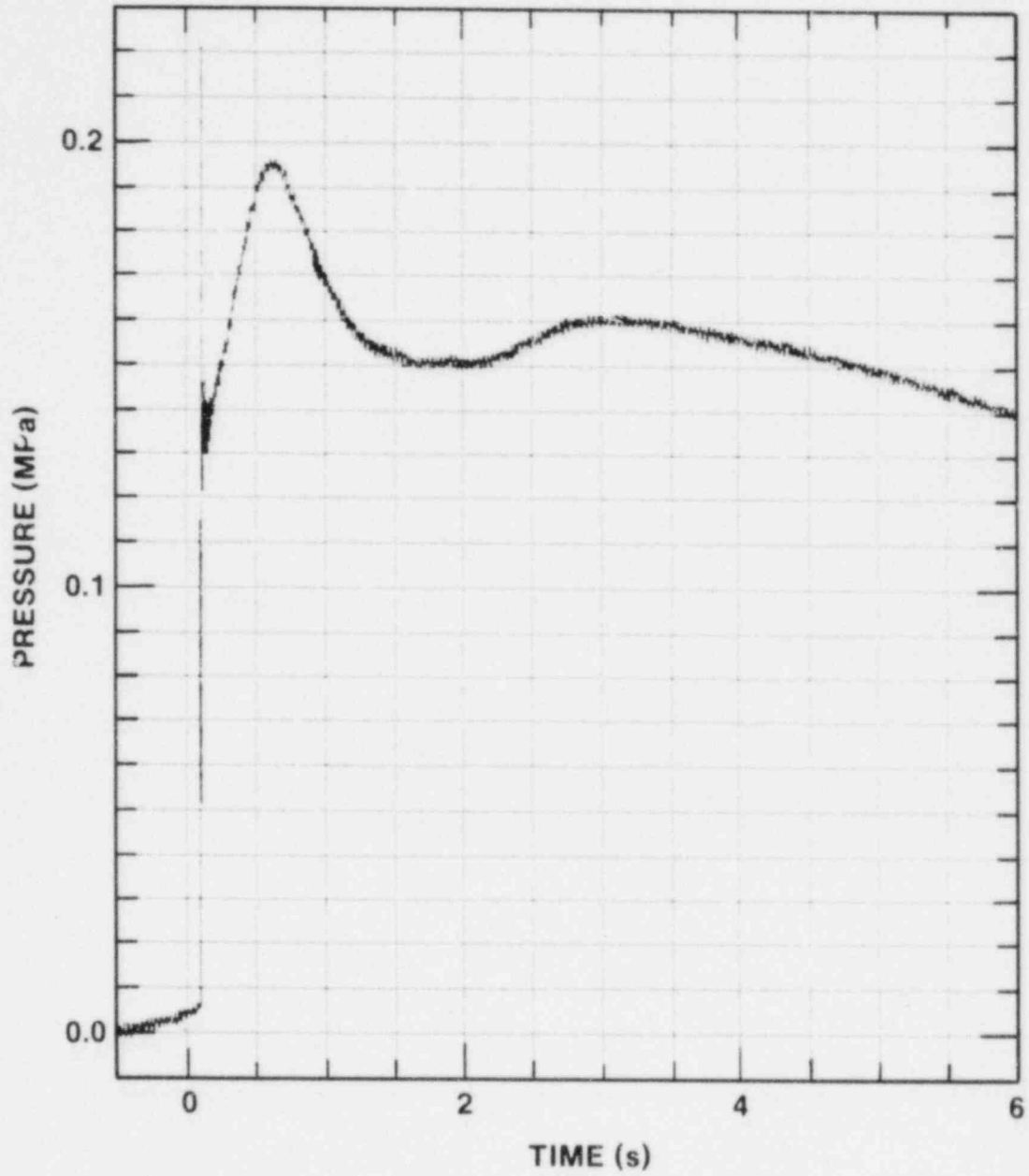Figure 6b.   FITS7B Chamber Air Pressure (expanded time scale)

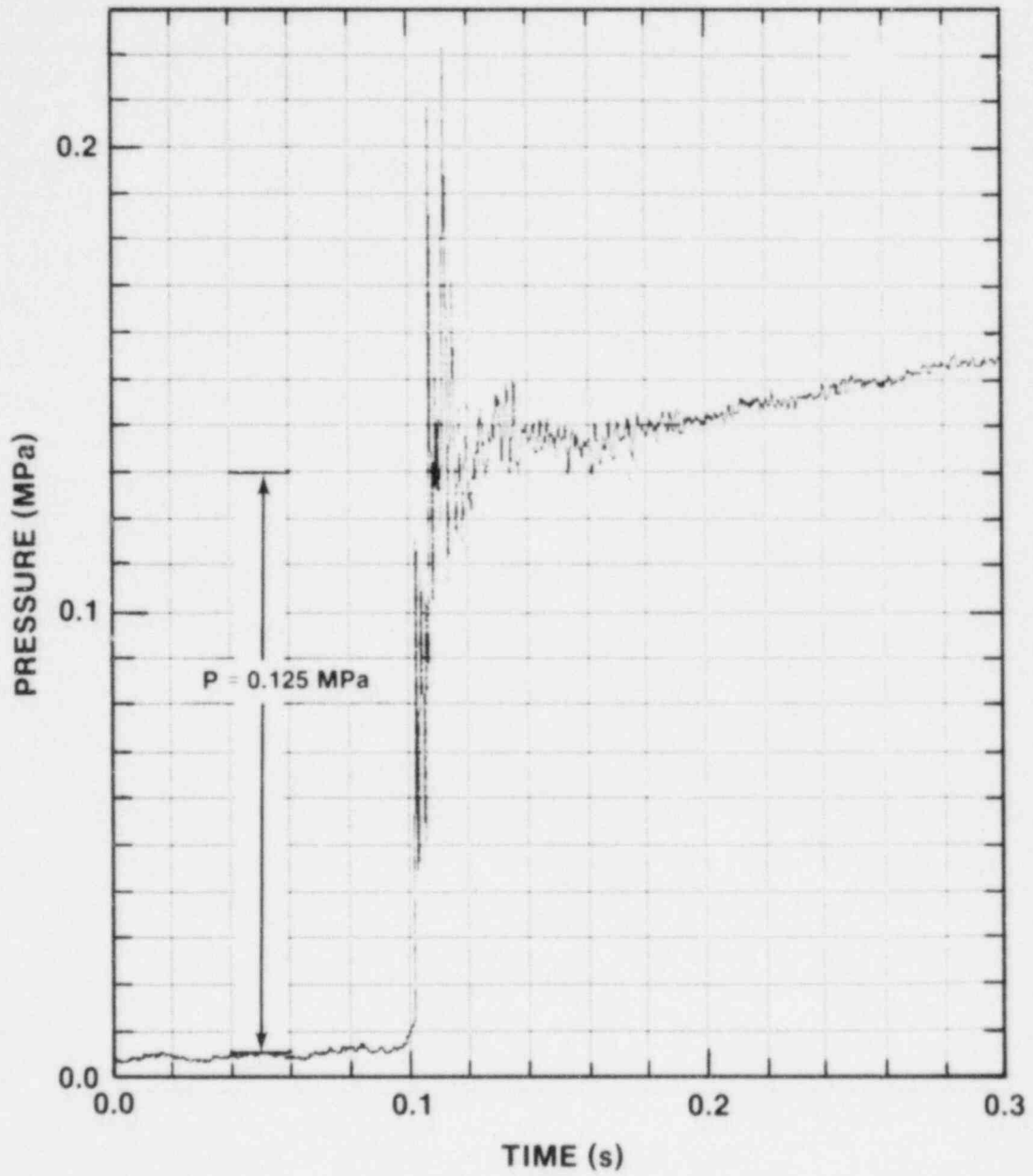Figure 7a.   FITS9B Chamber Air Pressure

-17-

Figure 7b. FITS9B Chamber Air Pressure (expanded time scale)

shown in Figures 8, 9, and 10. The first explosion in FITS1B occurred 142 ms after melt entry and was similar to the single explosions described above. We estimated that 14 kg of the total of 18.7 kg of melt was coarsely mixed in the water prior to triggering of the explosion at the melt-water interface on or near the water surface. The explosion was triggered before the submerged leading edge of the melt had contacted the water chamber base, and the direction of propagation was downward at approximately 300 m/s. Pieces of water chamber and residual water and melt impacted the camera ports before the second explosion, which was not immediately observed; this explosion became apparent only when pressure data became available. Comparison of pressure data and visual observations showed that there was a second explosion 133 ms after the first.

Chamber air pressure data (Figure 8) showed two peaks due to the steam explosions and two corresponding pressure plateaus, followed by a small late-time repressurization.

FITS4B and 8B were attempts to reproduce the FITS1B double explosion result and to determine if entry velocity and/or water depth were important initial conditions for a double explosion; the results, however, were quantitatively different from FITS1B. Only a small quantity of melt was in the water prior to a surface-triggered first explosion (~1.7 kg in FITS4B and ~1.9 kg in FITS8B). These explosions, although not recorded by the water phase transducers (~60 cm from the explosion site), were observed visually and were sufficiently energetic to cause the water chambers to fail; i.e., the walls and water began to move radially outward toward the camera ports.

Melt fragmentation and mixing in the residual water was enhanced by the first explosion. We observed that the melt was fragmented more thoroughly: there were more droplets, and they were typically in the 5 to 10 mm diameter range. In addition, the melt was more dispersed, and its velocity as it fell through the residual water was approximately twice that observed when no explosion occurred. The second explosion occurred at approximately the time the melt-water mixture contacted the water chamber base. Due to the severe geometry distortion caused by the first explosion, a propagating wave was not visually observed in either of these second explosions.

Air chamber pressure data for FITS8B (Figure 10) show the characteristics of this type of double explosion. At 27 ms after entry, the small, first explosion occurred that enhanced melt coarse mixing in the residual water. The result of this enhanced mixing was observed as a slow pressurization of the FITS chamber prior to the second explosion that occurred 146 ms after entry. Late-time pressurization
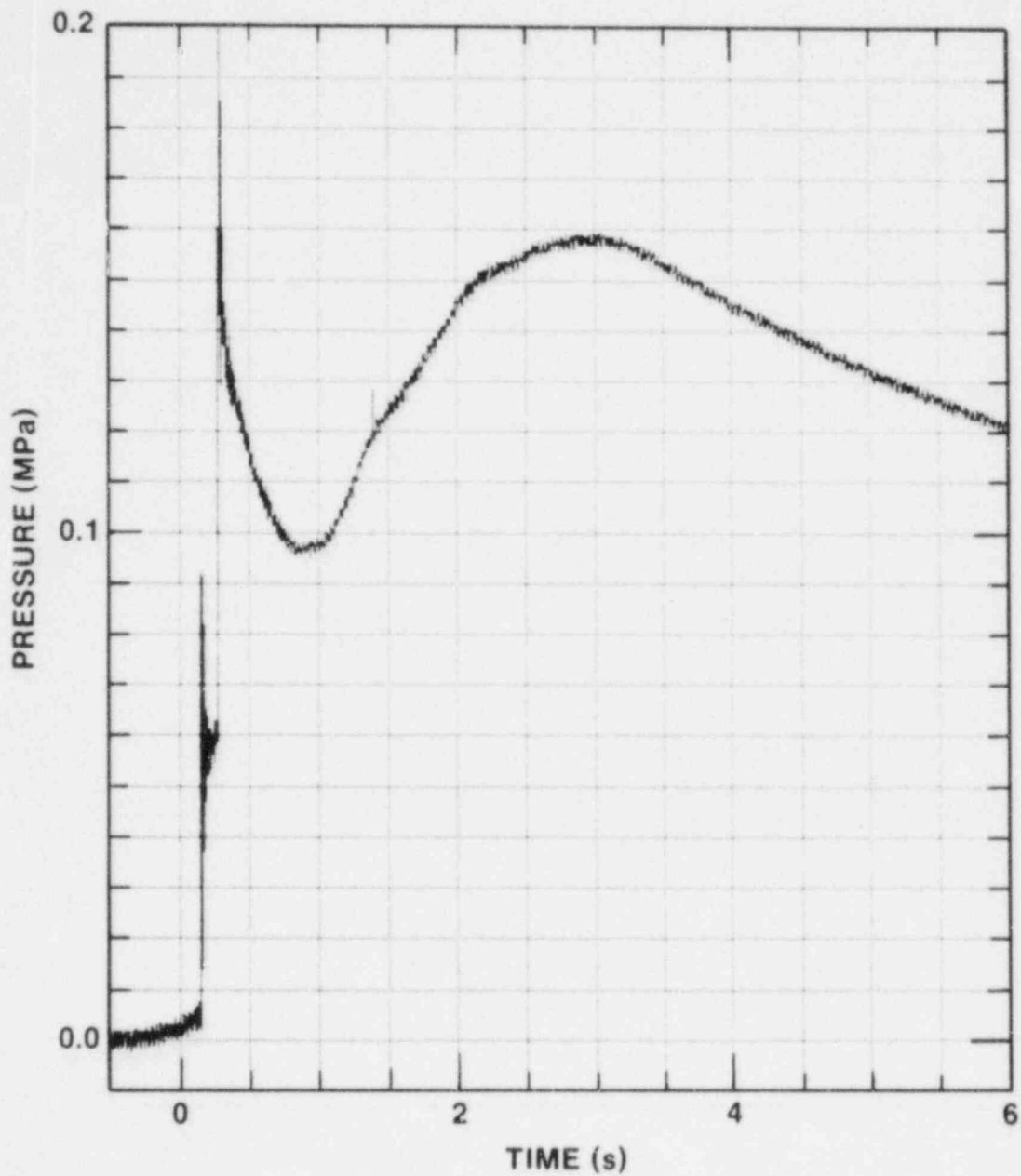
Figure 8a. FITS1B Chamber Air Pressure (two steam explosions separated by 143 ms. Second explosion not clearly observed visually.)
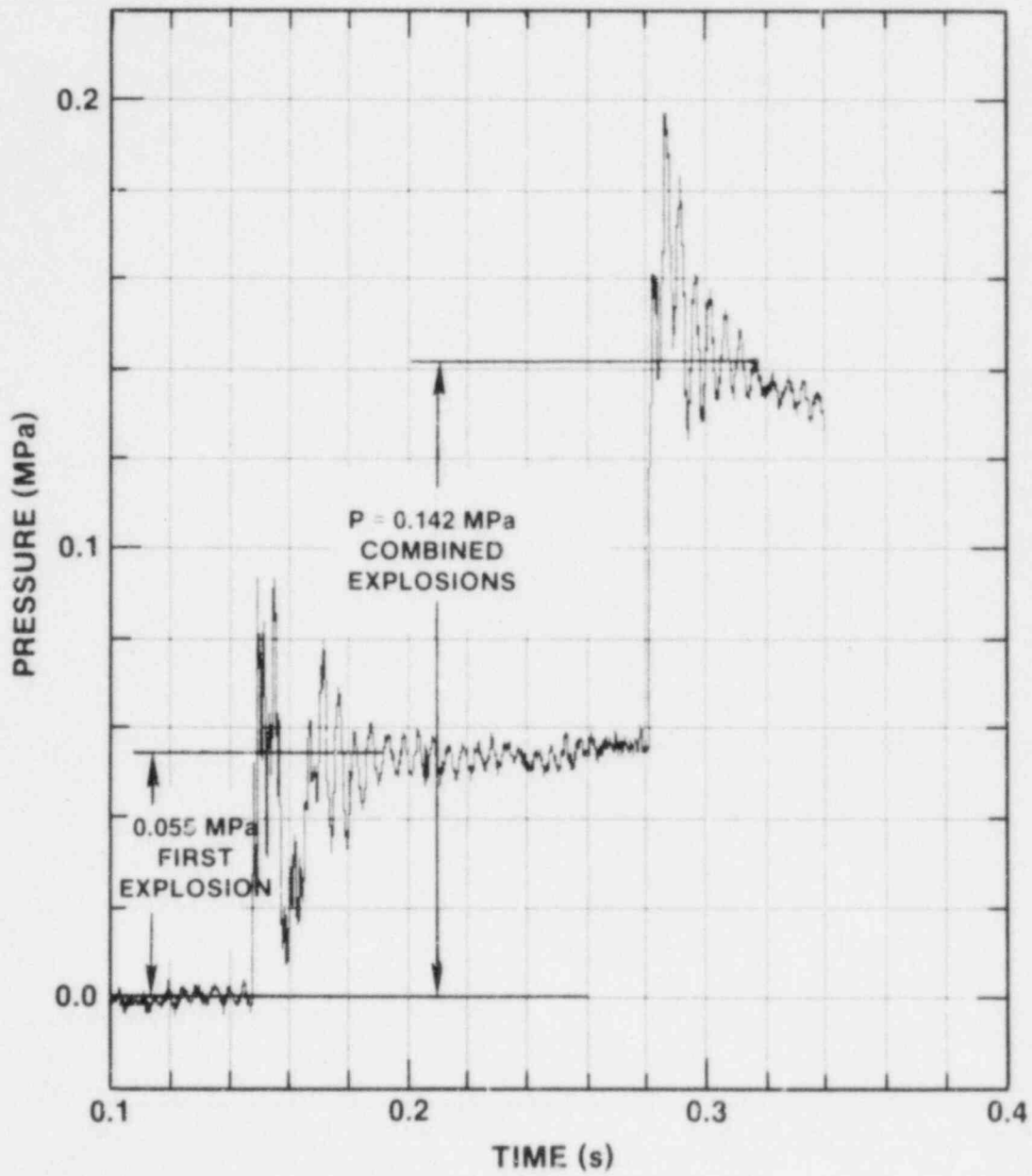
Figure 8b. FITS1B Chamber Air Pressure (expanded time scale)
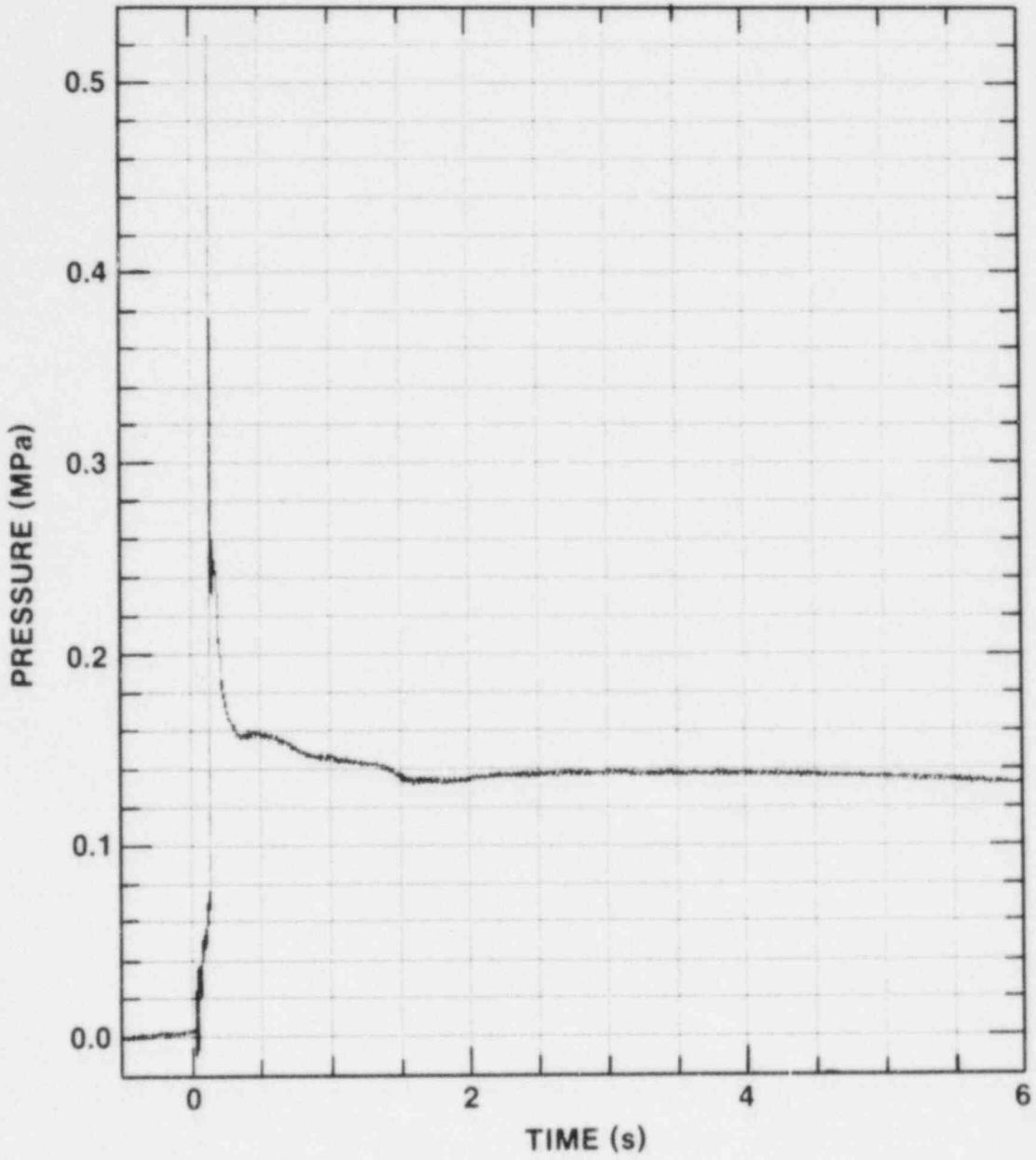
Figure 9a. FITS4B Chamber Air Pressure (two explosions)
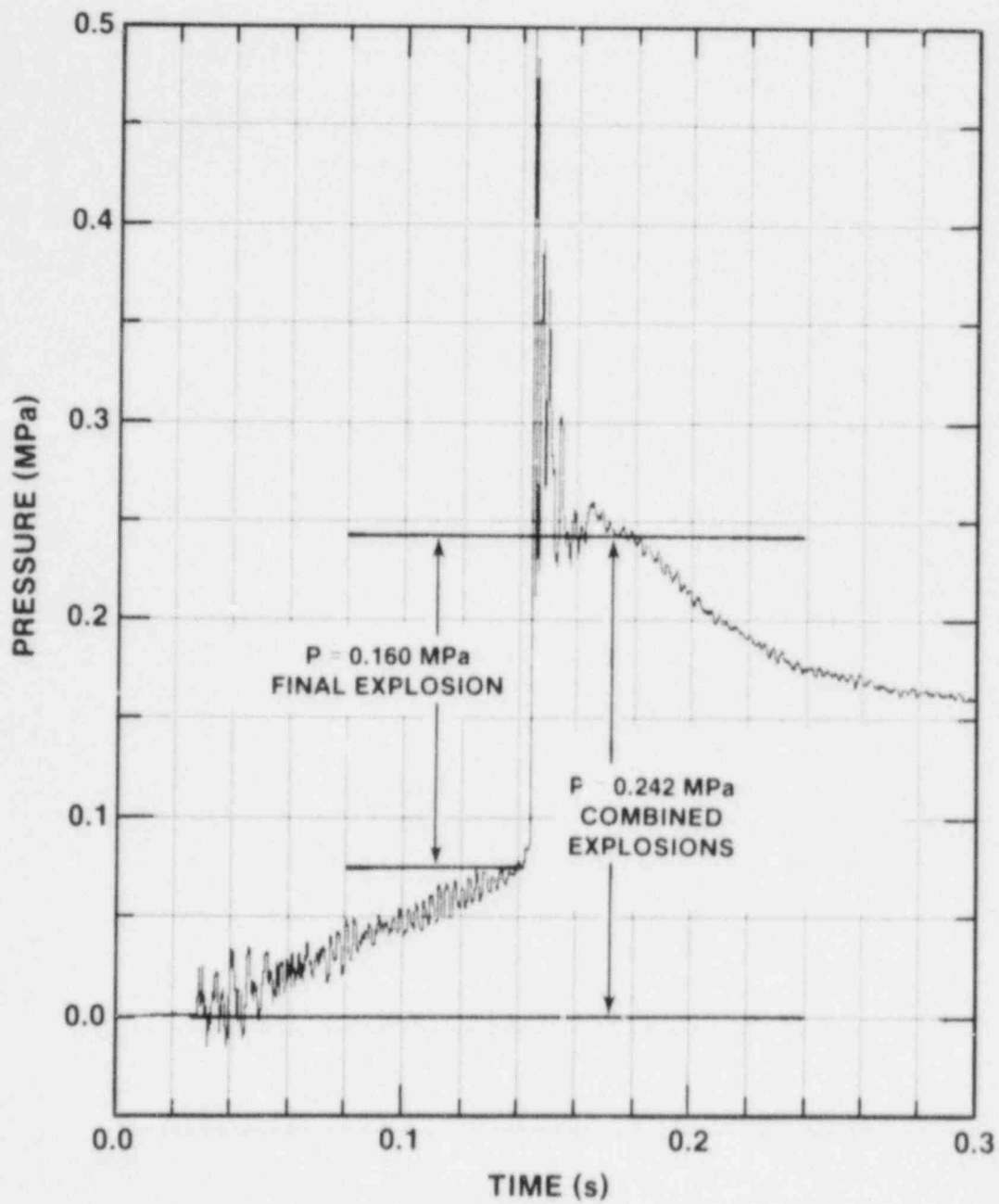
Figure 9b. FITS4B Chamber Air Pressure (expanded time scale)
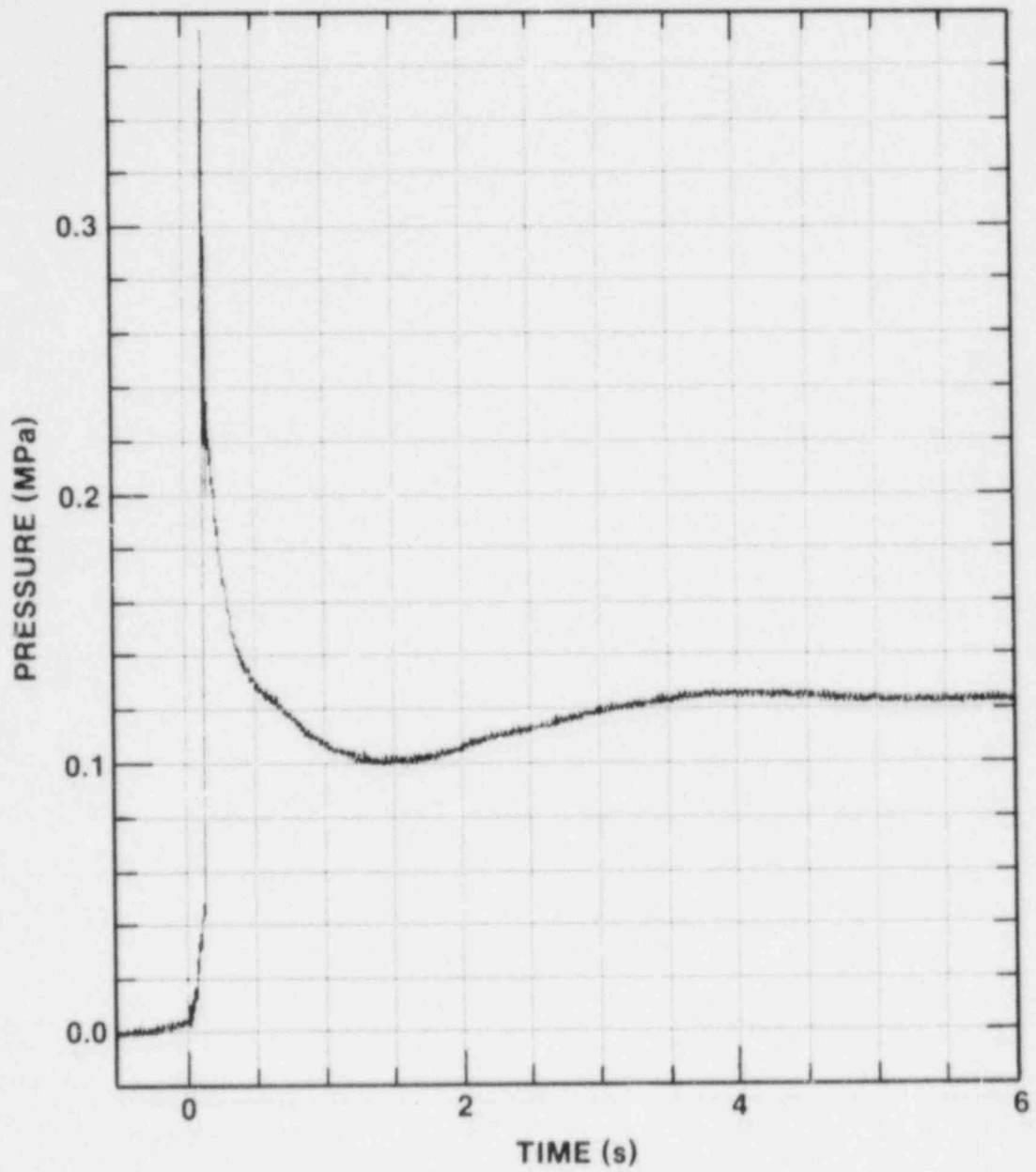
Figure 10a. FITS8B Chamber Air Pressure (two explosions)
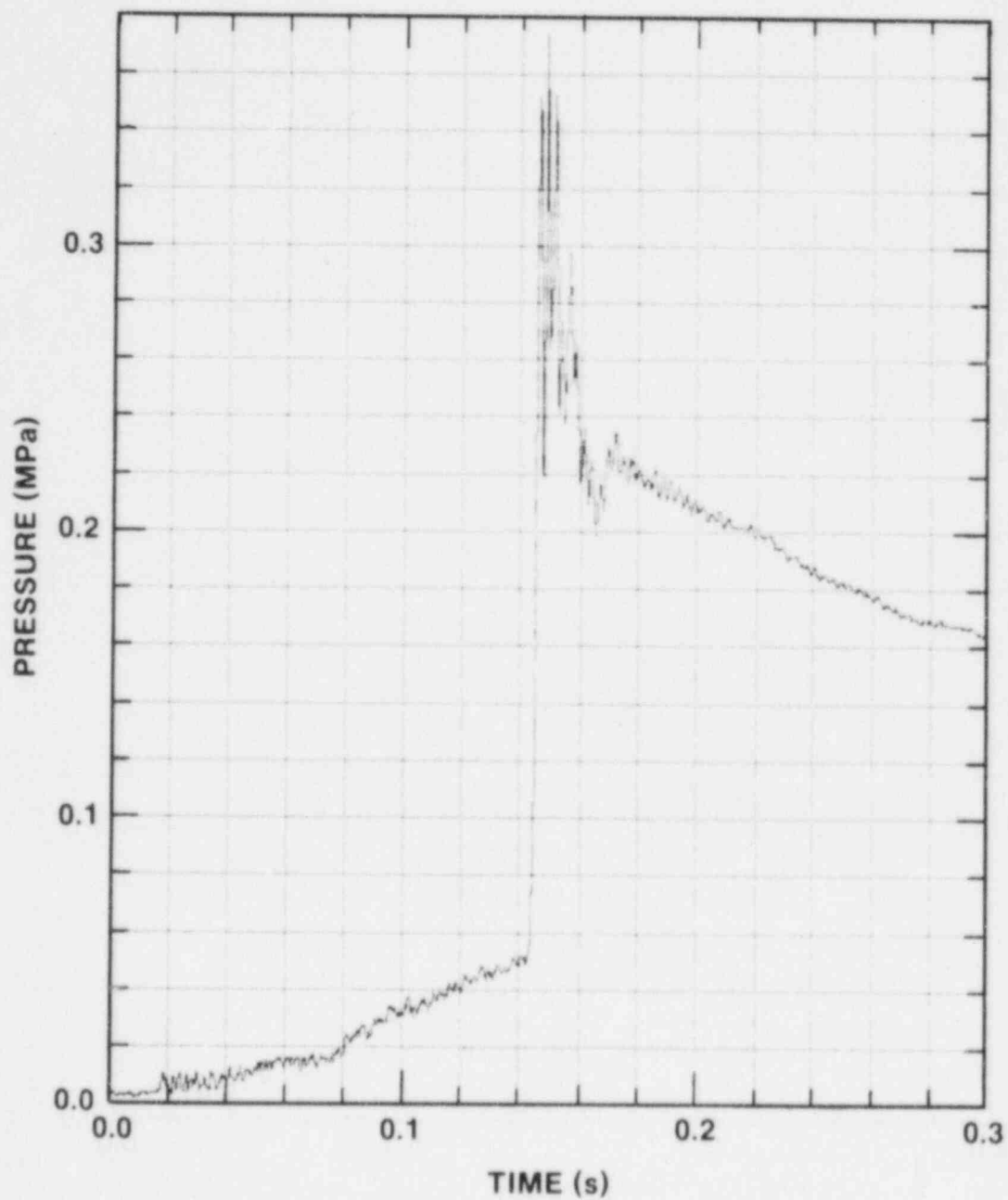
Figure 10b. FITS8B Chamber Air Pressure (expanded time
scale)

following the peak from this explosion was smaller than any others observed, indicating a more efficient explosive utilization of the melt thermal energy. Similar results were obtained from FITS4B.

3.4 Saturated Water Tests

Two experiments were done in saturated water. FITS5B resulted in a very late melt release due to a signal cable problem. No camera data were obtained. The melt was delivered approximately 70 s after thermite ignition (normal time averaged 20 s) and was probably cooler and more dispersed at water entry. No explosion resulted. Data from this experiment (debris, chamber pressure, and temperature) may be useful in studying steam spike behavior. FITS6B was a repeat of 5B and was a successful test. No explosion occurred, although four disturbances (as described earlier) were observed. None of these released sufficient energy to initiate the propagation phase. Figure 11 shows the air pressure data for this nonexploding experiment. A summary of the chamber air pressure data is shown in Table 2.
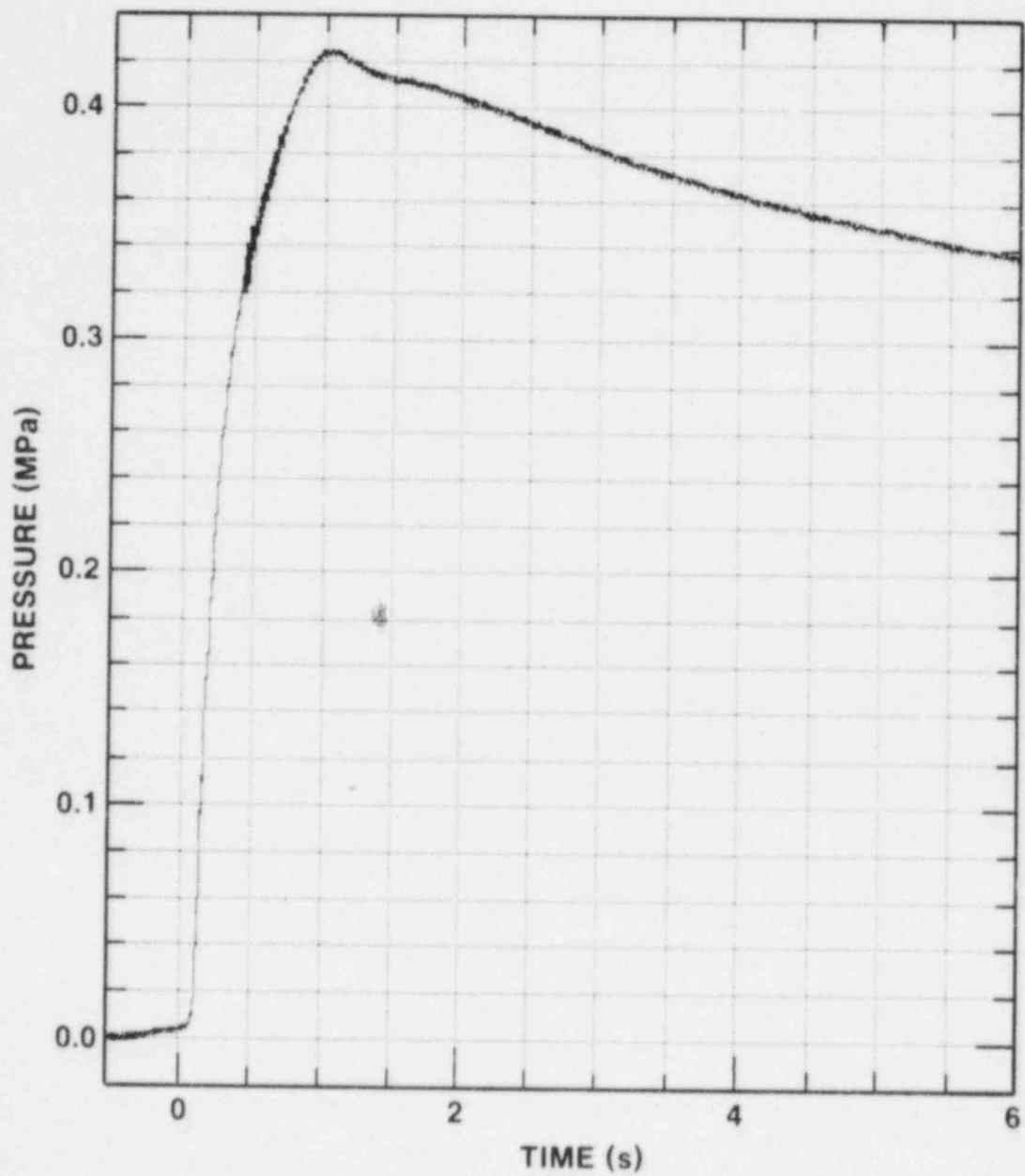
Figure 11a. FITS6B Chamber Air Pressure (saturated water)
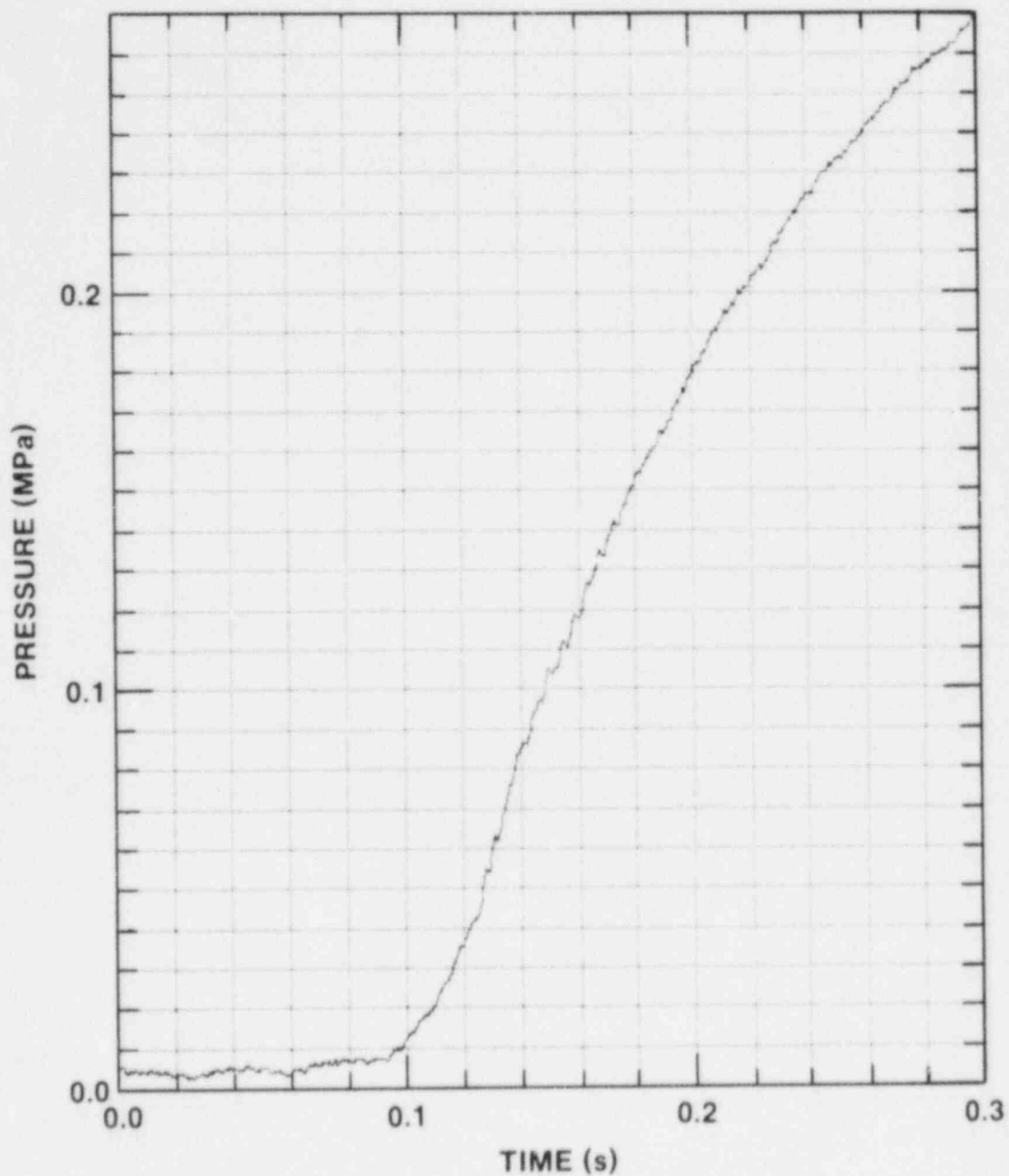
Figure 11b. FITS6B Chamber Air Pressure (expanded time
scale)

Table 2

Chamber Air Pressure Data Summary
(Times From Melt Entry)

Expt.	Steam Explosion Phase				Quasi-Static Pressure Plateau (MPa)		Steam or Hydrogen Phase	
	Explosion (s)		Pressure Peaks (MPa)				Time to Peak (s)	Peak Pressure (MPa)
	1st[a]	2nd	1st	2nd	1st	2nd		
1B	0.144	0.282	0.095	0.197	0.055	0.142	2.95	0.158
4B	0.029	0.146	0.020	0.500	n.o.[b]	0.242	4.00	0.138
8B	0.017	0.144	0.01	0.373	n.o.	0.215	3.95	0.126
2B	0.087	n.o.	0.220	n.o.	0.080	none	0.90	0.227
3B	0.081	n.o.	0.440	n.o.	0.115	none	1.00	0.500
6B	n.o.	n.o.	n.o.	n.o.	none	none	1.00	0.424
7B	±0.20	n.o.	0.01	n.o.	0.004	none	3.60[c] (1.20)	0.485 (0.425)
9B	0.102	n.o.	0.210	n.o.	0.125	none	4.00[c] (0.60)	0.160 (0.195)

[a] Time taken from start to pressure rise. Zero time taken from average of two active melt position sensors 2.5 cm above water surface.

[b] Not observed.

[c] Additional peaks observed in these two experiments that may be associated with steam or hydrogen production prior to debris settling to the FITS chamber base.

4. ENERGETICS OF THE INTERACTIONS

In a steam explosion, the conversion of melt thermal energy initially appears principally in two forms: the kinetic energy imparted to the liquid water initially adjacent to the fuel-coolant mixture explosion site, and the work done by the outwardly expanding high pressure vapor (involving a shock wave) on the compressible medium beyond the outer boundary of the water region. These two quantities are essentially independent. At later times, further energy exchange will occur when the liquid water and compressible medium become mixed. This new viewpoint, essentially energy conversion ratio partition, means that the total mechanical utilization of the rapidly transferred melt thermal energy is given to first order by

$$\eta_{tot}(t) = \eta_{KE}(t) + \eta_D(t)$$

with

$$\eta_{KE} = \frac{KE}{Q_m}$$

and

$$\eta_D = \frac{\Delta PV}{(\gamma - 1)Q_m}$$

where

Q_m = melt thermal energy

KE = kinetic energy

ΔP = chamber pressure increase

V = chamber volume

γ = specific heat ratio.

While the second equation for η_{KE} is self-explanatory, the development of the third equation for η_D requires discussion, as follows.

In the FITS lucite tank experiments, the partition of converted energy into these two terms may have a degree of

-30-

interdependence in the sense that the mass of water around the explosion source may have a tamping effect on the strength of the shock wave that compresses the outermost medium. In an actual reactor situation, the interdependence due to tamping may be greater because there is an increased degree of confinement from the walls of the Reactor Pressure Vessel (RPV) compared with the lucite tank.

For LWR safety considerations, the kinetic energy term may be related to water slug missile production, which may cause failure of the RPV head, while the shock wave through the water initially surrounding the explosion site may induce RPV bottom failure. The severity of these effects will probably be ameliorated to some extent since the propagation phase of the explosion takes finite time, which will limit the peak pressure available, and there will be an impedance mismatch between the water region and the RPV wall, which will result in reduced transmission of incident pressure waves.

For a better interpretation of the concept of conversion ratio in the FITS experiments, consider Figure 12a, showing the FITS chamber as containing only two distinct and separated substances, air and water, at ambient pressure, P_a, and ambient temperature T_a, for time $t < 0$. Let the boundary of system A enclose the water, and let system B be the air between the boundary of system A and the rigid chamber wall. Next, assume the heat, Q_e, is rapidly transferred from the melt and vaporizes part of the water at constant volume so that at time $t = 0$, system A (with the same volume as $t < 0$) contains two distinct and separated substances: steam at high temperature, T_e, and high pressure, P_e, and water (Figure 12b). It is also assumed that the residual liquid water is at pressure P_e but maintains the original ambient lower temperature, T_a. (After rapidly transferring thermal energy Q_e down to the thermal equilibrium temperature T_e, the melt is considered virtually removed from the total system, so that it plays no part in events for $t > 0$.)

At $t = 0$ (Figure 12b), system A starts an expansion process, and this gives kinetic energy to the water (shown schematically as four sectors in Figure 12c for $t > 0$) and does work in compressing the air in system B.

Considering the process for $t > 0$ to be adiabatic, conservation of energy E for system A requires

$$E_A = \left| -\int_i^f P\,dV \right|_A$$
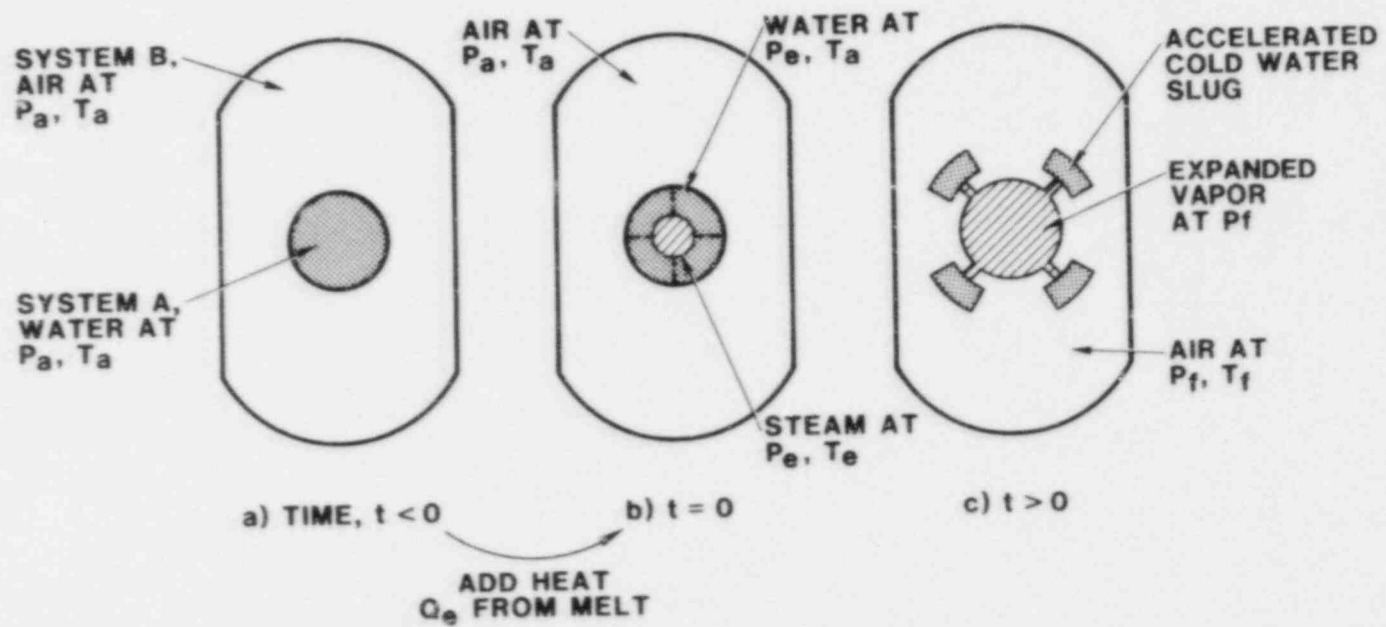
Figure 12. FITS Chamber System Boundaries

where V is volume and i and f stand for initial and final conditions, respectively.

For energy E assumed to contain only internal energy E_{int} and kinetic energy E_k,

$$\Delta E_A = [E_f - E_i]_A$$

$$= [E_{int,f} + E_{k,f} - (E_{int,i} + E_{k,i})]_A \quad .$$

The work done adiabatically by system A on system B will increase the internal energy of system B, so that

$$\left[\int_i^f PdV \right]_A = [MC_v(T_f - T_a)]_B$$

where M is the mass of air in system B with assumed constant volume specific heat $[C_v]_B$.

For simplicity, it will be assumed that gas and vapor motions for some $t > 0$ will be zero when $[P_f]_A = [P_f]_B$, so that only the water in system A will have kinetic energy, $[E_{k,f}]_A$.

Hence, from the above equations

$$[E_{int,i} - E_{int,f}]_A = [E_{k,f}]_A + [MC_v(T_f - T_a)]_B \quad .$$

Assuming for $t > 0$ that initially increasing just the pressure of the water from P_a to P_e in system A increases its internal energy by only a negligible amount, the last equation shows that the loss of internal energy of the high-pressure, high-temperature vapor source in system A produces kinetic energy in the water slug and, by compression, increases the internal energy of the chamber air. In other words, starting with all water in system A at some $t < 0$, addition of melt thermal energy Q_e by $t = 0$ results in the independent production of water slug kinetic energy and chamber pressurization. Hence, measurement of water masses and associated velocities and measurement of chamber air pressures (or preferably, as indicated below, chamber air temperatures) will indicate how the transferred melt energy Q_e has been utilized.

The various assumptions used above contain some major approximations, but the principal result will still stand, and it is possible to maintain rigorously the concept of

-33-

system boundaries and contained, identifiable matter. Deviations in the actual situation will occur, for instance, because for t > 0, the melt will continue transferring heat in cooling to a temperature below T_e during the vapor expansion phase, and the rapidity of events in the presence of strong shock waves will not result in a simple, uniform gas phase zero velocity condition at the assumed pressure condition $[P_f]_A = [P_f]_B$. Another deviation will occur because the water slug will take up sensible heat not accounted for above, but, in principle, appropriate mass averages could be established with proper energy accounting to give an equivalent cold water slug mass and a mass of high-energy vapor for the start of expansion at t = 0. In any case, from the experimental point of view, these intermediate steps are not required, since the energetic effect of interest of putting melt into coolant can be determined in principle with fair accuracy by measurement of water masses and velocities, and chamber air effects. Practical difficulties arise in making and interpreting these measurements. The internal energy increase in the chamber air is

$$E_B = [MC_V(T_f - T_a)]_B = \left[\frac{P_f V_f - P_a V_i}{\gamma - 1}\right]_B$$

where γ is the specific heat ratio for air, and an assumed perfect gas equation of state for air has been used. For earlier FITS experiments, it was assumed the $[V_f]_B \approx [V_i]_B$, so that

$$\Delta E'_B = \left[\frac{\Delta P V_i}{\gamma - 1}\right]_B$$

where

$$\Delta P_B = [P_f - P_a]_B \quad.$$

Use of this expression for $\Delta E'_B$ overestimated the internal energy change since $[V_f]_B < [V_i]_B$. However, measurement of temperature change coupled with mass of air (known by system definition) gives a more accurate indication of E_B without the need to determine $[V_f]_B$. In analogy with one-dimensional shock tube operation, the temperature $[T_f]_B$ should be measured with fast response (~10 µs) instrument located towards the top of the chamber. In principle, the arrival of the shock wave (which outruns the contact surface separating the expanding water vapor from the air being compressed) would cause a temperature jump and induce air motion

(and thus kinetic energy). The shock system reflected from the chamber top would reduce the air approximately to rest with further temperature increase, and this temperature (the stagnation value) would be the most appropriate value to use for $[T_f]_B$ before the arrival of water vapor at the contact surface. The instrument should be installed in such a way that it would measure this stagnation temperature (rather than a value related more to the so-called recovery temperature). In practice, the best-measured value to use for a stagnation temperature would probably be the highest value recorded in close time proximity (~20 µs) to the observed arrival of the shock wave, assuming the instrument has properly stagnated the flow at the sensor head. Deviations from this ideal condition would occur because the shock wave has spherical characteristics rather than being planar, and there would be a complicated reflection system from the hemispherical head of the FITS chamber.

Following the above, the energy released in the steam explosion in the FITS experiments was calculated in two parts. The first part used the quasi-static pressure plateaus recorded by the FITS gas phase pressure transducers and was related to the amount of work stored in the gas phase due to the liberation of energy from the steam explosion by shock wave propagation. The concepts used in this calculation were taken from classical chemical explosion theories. The value that resulted is not directly applicable to assessing damage potential from a steam explosion in terms of missile generation.

Because these measurements were based on chamber responses due to shock wave reverberations and debris expansions, and occur at times on the order of tens of ms after the explosion, effects of water mass and amount of fuel present affect the measurement. That is, chamber pressure was affected by the heat transfer from melt unquenched in the rapid propagation phase to the remaining water. Nonetheless, this calculation was felt to be an indication of part of the strength of the explosion as it was affected by other experimental parameters, such as mass ratio, water depth, and geometry, and could affect LWR safety issues related to containment damage due to overpressurization.

The second part of the energy release was directly related to the damage potential of a steam explosion due to debris acceleration. For this part, measurements of debris velocities and estimates of accelerated masses were used to calculate kinetic energy. These measurements were made within 1 to 2 ms after the explosion trigger and were not affected by heat transfer effects from unquenched fuel to coolant to as large a degree as the previous part of the calculations based on chamber pressures.

In-chamber experiments (FITSA and B) were used to calculate conversion ratios (η_D) that are analogous to heats of detonation. Since EXO-FITS experiments (MD, MDC) did not allow that type of calculation to be done because the expansion volume was infinite, only a conversion ratio based on kinetic energy (η_{KE}) was possible. In some cases (FITSA and B), both calculations could be done.

A summary of the data available for conversion ratio calculation is shown in Table 3. The conversion ratios were based on the total melt mass delivered; in FITSB experiments that quantity was typically 18.7 kg. It is clear from the photographic observations, as well as from debris distributions, that not all the melt was involved in the explosion. Since at this time there is no precise way of estimating that quantity, the total fuel mass was used as the basis. (This, of course, implies a nonconservative estimate of conversion ratio; i.e., based on mass of fuel interacting, the conversion ratio would be larger than these estimates.)

4.1 Conversion Ratios Due to Chamber Pressure Rise

FITS chamber air pressure gauges (Figures 4 through 11) were used to calculate a conversion ratio by estimating the hydrostatic pressure that appeared as a pressure plateau following the sharp pressure spikes produced by the explosion. These plateaus, shown in Table 2, persisted for times on the order of tens of milliseconds before thermal energy from the unreached melt could increase the gas phase pressure, or condensation effects could decrease it. The plateau pressures used were those observed between 10 and 30 ms after the start of the steam explosion spike.

Three sample calculations are shown below to demonstrate the method: the first is from a single-explosion event (FITS9B) and the second and third from the double-explosion events (FITS1B and 4B). The following parameters were held constant for the calculations:

1. Chamber volume, 5.6 m^3. No correction for decreases in volume due to water, steam, or hydrogen;

2. Ratio of specific heats, $\gamma = 1.3$;

3. Fuel thermal energy, $C\Delta T = 2.8$ MJ/kg.

4.1.1 FITS9B (Single Explosion)

Fuel mass = 18.7 kg

Thermal energy stored, $Q_m = 52.4$ MJ

-36-

Table 3

Summary of Data Available for
Conversion Ratio Calculations
(Nonexploding Events Omitted)

Expt.	Debris Velocity		Water Chamber Pressure Hist.		FITS Chamber Pressure History	Comments
	Radial	Axial	Wall	Base		
MD8	X	–	–	–	–	EXO-FITS Fe/Al_2O_3
11	X	–	–	–	–	EXO-FITS Fe/Al_2O_3
14	X	–	–	–	–	EXO-FITS Fe/Al_2O_3
15	X	–	–	–	–	EXO-FITS Fe/Al_2O_3
16	X	–	–	–	–	EXO-FITS Fe/Al_2O_3
18	X	–	X	X	–	EXO-FITS Fe/Al_2O_3
19	X	–	X	X	–	EXO-FITS Fe/Al_2O_3
MDC2	X	–	X	–	–	EXO-FITS corium
14	X	–	–	–	–	EXO-FITS corium
16	X	–	X	–	–	EXO-FITS corium
17	X	–	X	X	–	EXO-FITS corium
FITS2A	–	–	–	–	–	Partial reaction – no data
3A	X	–	–	–	X	5 kg Fe/Al_2O_3
5A	–	–	–	–	X	5 kg Fe/Al_2O_3
1B	X	X	X	–	X	18.7 kg Fe/Al_2O_3
2B	X	X	–	X	X	18.7 kg Fe/Al_2O_3
3B	–	X	X	X	X	18.7 kg Fe/Al_2O_3
4B	X	X	–	X	X	18.7 kg Fe/Al_2O_3
7B	–	X	X	–	X	18.7 kg Fe/Al_2O_3
7BR	X	–	X	X	–	EXO-FITS 18.7 kg
8B	–	X	X	X	X	18.7 kg Fe/Al_2O_3
9B	X	X	X	X	X	18.7 kg Fe/Al_2O_3

Pressure rise to plateau, $\Delta P = 0.125$ MPa

Energy required to pressurize chamber:

$$Q_D = \frac{PV}{\gamma - 1} = \frac{(0.125 \times 10^6)(5.6)}{0.3} = 2.33 \text{ MJ}$$

Conversion ratio η_D

$$\eta_D = \frac{Q_D}{Q_M} = \frac{2.33}{52.4} = 0.044 \quad .$$

4.1.2 FITS1B (Double Explosion)

Pressure records from this experiment were unique inasmuch as two plateau-pressures were observed as shown in Figure 8b. Conversion ratios (η_D) were calculated in two ways. In the first calculation, the first pressure plateau and an estimated fuel mass (based on entry velocity and shape) were used to calculate the conversion ratio. The second calculation used the total fuel mass delivered and the total pressure rise to the second plateau.

a. First explosion

Fuel mass = 14 kg (estimated)

Thermal energy $Q_m = 39.2$ MJ

Pressure rise to first plateau, $\Delta P = 0.055$ MPa

Pressurizing energy, $Q_D = 1.02$ MJ

Conversion ratio, $\eta_D = \frac{1.02}{39.2} = 0.026 \quad .$

b. Combined explosion

Fuel mass = 18.7 kg

Thermal energy $Q_m = 52.4$ MJ

Plateau pressure = 0.142 MPa (total pressure rise)

$Q_D = 2.65$ MJ

Conversion ratio, $\eta_D = \frac{2.65}{52.4} = 0.051 \quad .$

4.1.3 FITS4B (Double Explosion)

Two explosions were observed in this experiment, the first, 29 ms after melt entry, and the second, 146 ms after entry, as shown in Figure 9b. The energy released from the first explosion could not be estimated using the method described because no steam explosion spike or plateau pressure was recorded. Instead, we observed the effect of the first explosion in the enhancement in melt fragmentation prior to the major second event. The pressure ramp was due to surface area enhancement of the melt by the first explosion, which resulted in more rapid steam and hydrogen generation rates. This steam production increased the chamber ambient pressure by 0.082 MPa. The major (second) explosion occurred in the chamber at this elevated pressure. The plateau pressure used for this calculation was the change in pressure (ΔP) from the end of the ramp to the plateau pressure. A second calculation was done using the total pressure rise.

a. <u>Conversion ratio for (ΔP) of second explosion</u>

Fuel mass = 18.7 kg

Thermal energy Q_m = 52.4 MJ

ΔP = 0.160 MPa (end of ramp to second plateau)

Pressurizing energy, Q_D = 2.98 MJ

Conversion ratio, $\eta_D = \dfrac{2.98}{52.4} = 0.057$.

b. <u>Combined explosion (total pressure rise)</u>

Fuel mass = 18.7 kg

Thermal energy Q_m = 52.4 MJ

Pressurizing energy (Q_D)

Q_D = 4.52 MJ

Conversion ratio, $\eta_D = \dfrac{4.52}{52.4} = 0.086$.

Table 4 describes the conversion ratios calculated using the method described above.

4.2 Conversion Ratios Due to Kinetic Energy Produced

A direct measurement of the kinetic energy produced in a system can be calculated if the various masses and their associated velocities can be measured. The ability to do

Table 4

Conversion Ratios (η_D) Using FITS Chamber Pressure Histories

Expt.	Melt Mass (kg)	Melt Energy (MJ)	Press. (MPa)	Expl. Energy (MJ)	Conv. Ratio (η_D)	Comments
1B	14	39.2	0.055	1.02	0.026	First explosion
	18.7	52.4	0.142	2.67	0.051	Combined explosion
2B	18.6	52.1	0.080	1.49	0.028	
3B	18.6	52.1	0.115	2.14	0.040	
4B	18.7	52.4	0.160	2.98	0.057	ΔP, ramp to plateau
			0.242	4.50	0.086	Total pressure rise
7B[a]	12.0	33.6	0.004	0.08	0.002	
8B	18.7	52.4	0.165	3.09	0.059	ΔP, ramp to plateau
			0.215	4.03	0.077	Total pressure rise
9B	18.7	52.4	0.125	2.33	0.044	
3A[b]	5.3	14.8	0.012	0.22	0.015	
			0.040	0.74	0.050	
5A	5.4	15.1	0.020	0.27	0.018	

[a] Melt mass involved estimated from posttest debris.

[b] Pressure measurement affected by premature chamber venting; two bounds given.

this depends on the geometry of the system; i.e., can masses be accelerated such that the velocities can be measured accurately? In the FITS and MD experiments, this was not the case because of the design of the experiment. The debris velocity and mass distributions were three-dimensional, and accurate measurements were difficult to obtain. However, since it is important at least to bound the conversion ratio, and considering that a commonly accepted definition of conversion ratio uses mechanical work delivered, an attempt was made to estimate the conversion ratio based on kinetic energy calculations. In addition, two-dimensional codes can be used to study the interactions if some estimate of wall velocity and water phase pressure are available.

Kinetic energy delivered by the explosion can be estimated from both MD series and FITS series experiments. Available data include:

1. Water chamber wall velocity from:

   a. High-speed cameras.

   b. Water chamber wall pressure vs. time.

2. Water chamber base pressure histories from "rigidly" mounted base pressure gauges.

3. Water-debris slug velocity from:

   a. High-speed cameras (MD-series).

   b. Upper FITS chamber head pressure gauges.

4. Melt-water mixture average diameter prior to the explosion trigger.

5. Initial dimensions and masses.

Calculation of kinetic energy requires that two quantities be known: (1) velocity of a given mass and (2) the mass itself. For these experiments, velocities were either measured directly or were calculated from water chamber pressure-time data.

4.2.1 Velocity Measurements

The method used to calculate water chamber wall velocity is described below. Experiment FITS9B is used as an example because the data from this experiment were more reliable; i.e., wall velocity was also measured using high-speed cameras. Pressure-time records were numerically integrated to calculate the impulse delivered to the lucite chamber wall. Since the wall is intimately in contact with the

-41-

water, the wall impulse is a good indicator of initial water and debris velocity.

4.2.2 Wall Velocity Calculation from Pressure Histories

The following relations are used:

$$\int Pdt = \frac{mV}{A}$$

and

$$I = \rho \delta V$$

where

$$\int_{t_{exp}}^{t_{fail}} Pdt = I = \text{integrated pressure time history from wall transducer}$$

t_{exp} = time of explosion

t_{fail} = time where gauge appears to fail (assumed)

ρ = water chamber wall density, 1.18 g/cm^3

δ = water chamber wall thickness, 0.635 cm

V = calculated velocity from impulse measurement.

In this experiment, two wall pressure transducers were located on adjacent walls. A visual measurement of chamber wall velocity was made of a third wall (Figure 13).

A comparison of calculated wall velocity and measured velocity is shown in Table 5 and can be taken as typical of all the experiments.

It can be seen that calculations of wall velocity by the impulse method bound the actual camera value. The low value for velocity from gauge 2 was a result of early gauge failure; i.e., the total integration time was 1.5 ms versus 2.6 ms for gauge 1. When camera data are available, they are reduced for the required velocities, and impulse measurements are used as a check. In some cases, there are no camera data, as in FITS7B. In this case, an average integrated impulse was used to determine velocity. It is entirely possible that each of the walls had a different velocity due to lack of symmetry in a given experiment.
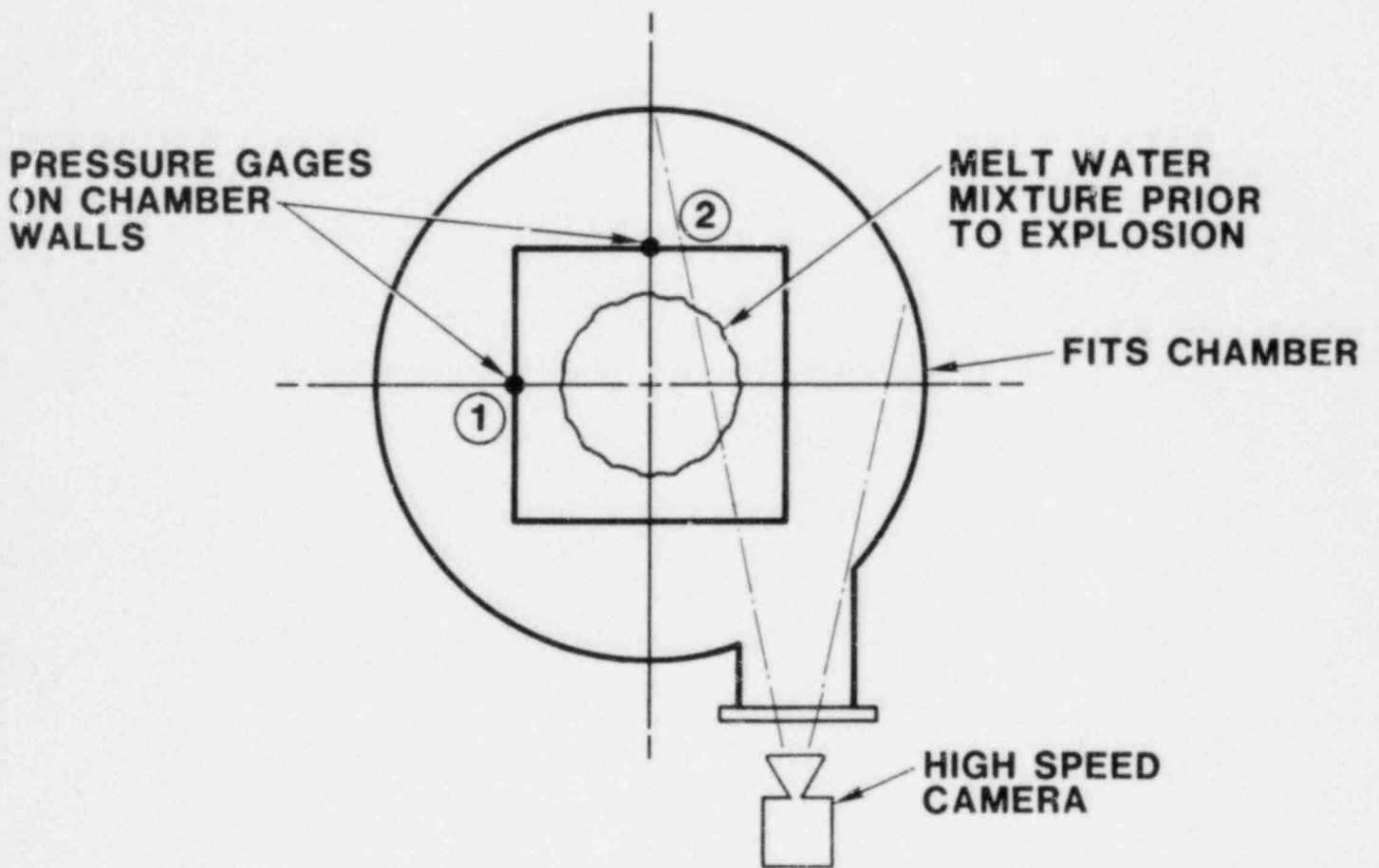
Figure 13. Chamber Wall Measurements

MD series experiments done EXO-FITS show that individual wall velocities for a given experiment agree within 20 percent, indicating that the best velocity to use is the visual one, at least at this time.

Table 5

Wall Velocity FITS9B

Method	Velocity	Percent of Camera Vel.	Total Integration Time for Impulse
Gauge 1 impulse	11,300 cm/s	118	2.6 ms
Gauge 2 impulse	5,700 cm/s	59	1.5 ms
Camera	9,600 cm/s	100	--

Visual observations show that most of the mass was contained in an expanding cylindrical region, at least early in time (volume expansion ~4 times). However, it was also observed that there was a vertical component of velocity that could also affect the kinetic energy. This velocity was measured in the FITS chamber by using upper-chamber head pressure gauges to record average velocity of debris driven by the explosion (Figure 14).

Experiments done EXO-FITS do not have a direct measure of this velocity since we concentrated on the mixture zone in these experiments with the high-speed cameras.[9] However, estimates of debris velocity could be made with pressure gauges located in the water chamber base, as described later.

4.2.3 Mass Estimation

This quantity is the most difficult to determine because of the experimental method; i.e., weak confinement that allows expansion in all directions. In order to estimate the masses involved the following assumptions were made:

1. The water chamber wall and surrounding water moved as a coherent mass during the time of measurement, and only the water surrounding the melt-water mixture was the mass used.

2. The vertical slug of debris moved as a coherent mass at the average velocity.

HEAD GAGES

DISTANCE TO HEAD GAGES

FITS CHAMBER

CENTER OF EXPLODING MASS
AT t = 0
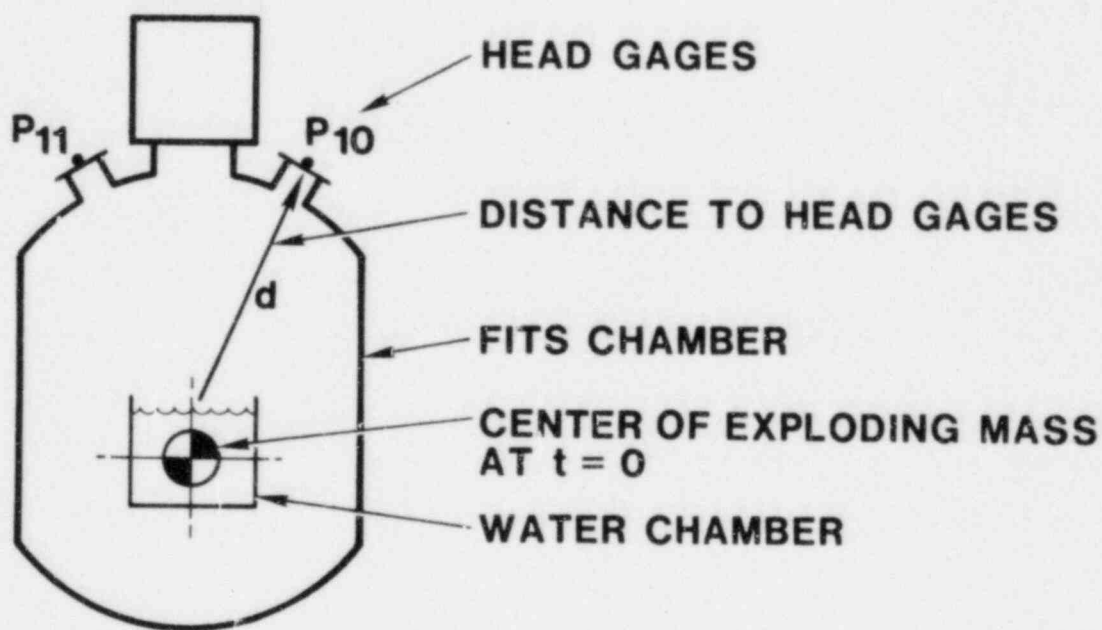
WATER CHAMBER

P_{11} P_{10}

d

Figure 14.   Debris Slug Average Velocity Measurement

3. The lateral expansion was cylindrical; i.e., each wall moved at the average velocity calculated by impulse measurements or as visually measured with high-speed cameras.

4. No mass was accelerated downward.

Assumption 1 results in lower than actual mass because some of the water-melt mixture also expanded. Assumption 2 will result in a lower than actual mass because the method used for mass estimation relies on average velocity, and the distance that the debris has to travel will be smaller than initially because some mass may already be in motion vertically prior to the explosion. Hence, it has an initial velocity and is closer to the upper head transducers. Assumptions 3 and 4 are reasonable, based on visual observations from the experiments. A visual representation of the assumptions is shown in Figure 15.

The method for estimating the lateral mass is given by the following and Figure 16

$$M_L = \rho_w (V_I - V_m)$$

where

ρ_w = water density

V_I = initial water volume

V_m = volume occupied by the melt-water mixture

and

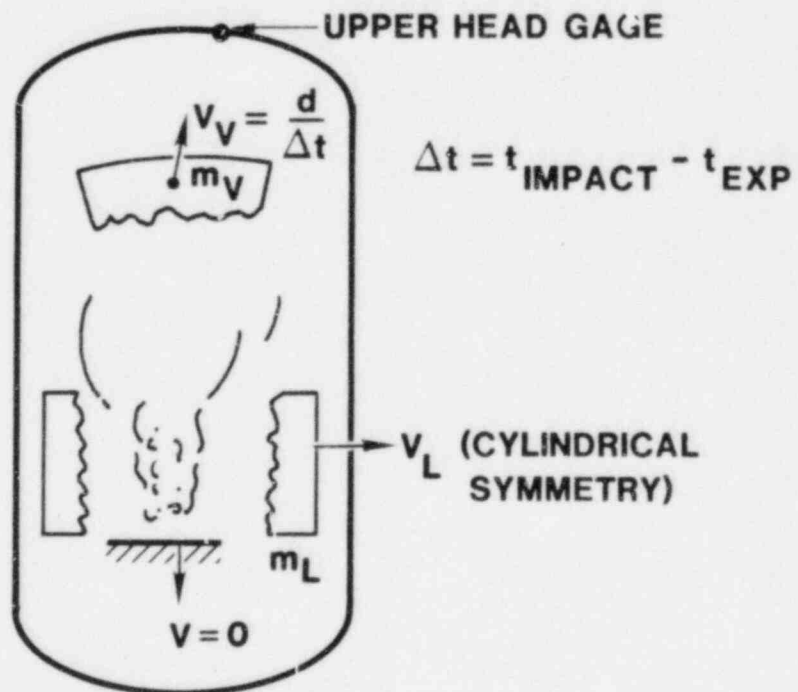$$V_m = \frac{\pi D_m^2}{4} h$$

where

h = water depth including level swell

D_m = measured melt-water mixture average diameter.

The vertical mass component estimation was based on two measurements: the average debris slug velocity (Figure 13 and 14) and the water chamber base pressure-time histories. These two data were used in the following way to estimate the vertical mass.
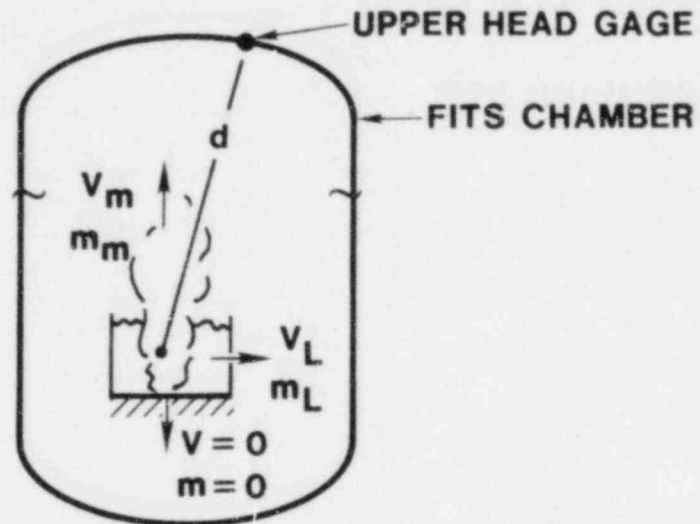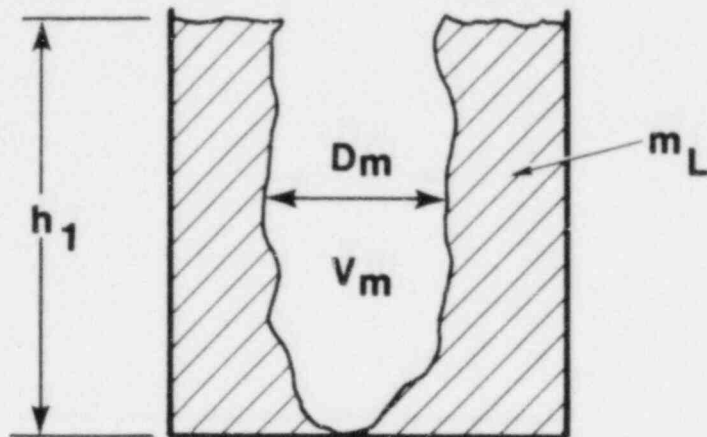
Figure 15. Visual Representation of Assumptions

Figure 16. Lateral Mass Estimation

$$M_V = \frac{IA}{V_V}$$

where

I = $\int p\,dt$ averaged from a maximum of three base transducers

A = Water chamber base area

V_V = Average debris slug velocity from initial distance and transit time from explosion (Figures 14 and 15).

The kinetic energies are then calculated by

$$KE_T = KE_V + KE_L$$

where

$$KE_V = \frac{1}{2} M_V V_V^2$$

$$KE_L = \frac{1}{2} M_L V_L^2 \quad .$$

4.2.4 Sample Calculation

A sample calculation using the above method is shown below, using data from FITS9B.

Lateral Direction

$$V_L = 9600 \text{ cm/s from cameras}$$

$$D_M = 35.6 \text{ cm}$$

$$\eta_M = 51.6 \text{ cm}$$

$$V_M = 51,362 \text{ cm}^3$$

$$V_I = 171,166 \text{ cm}^3$$

$$M_L = 119,804 \text{ g}$$

$$KE_L = \frac{1}{2}(119,804)(9600)^2 = 0.55 \text{ MJ}.$$

Vertical Direction

$$I = 60.3 \times 10^3 \text{ dyne-s/cm}^2$$

$$A = 61^2 \text{ cm}^2 = 3721 \text{ cm}^2$$

$$V_V = \frac{d}{\Delta t} = 9460 \text{ cm/sec}$$

$$M_V = 23,718 \text{ g}$$

$$KE_V = \frac{1}{2}M_V V_V^2 = 0.11 \text{ MJ}.$$

Total kinetic energy

$$KE_T = 0.66 \text{ MJ}.$$

Conversion ratio

$$Q_M = (18.7)(2.8) \quad 52.4 \text{ MJ}$$

$$\eta_{KE} = \frac{0.66}{52.4} = 0.013.$$

Conversion ratios (η) were calculated assuming that the total melt mass delivered was involved in the explosion, since it is not evident from debris distributions what melt mass was involved, especially in the cases where two separate explosions occurred. The values for η_{KE} and η_D obtained from the experimental data are shown in Table 6.

-49-

Table 6

FITSB Steam Explosion Results

Expt.	Initial Mass Ratio M_c/M_f	Water Volume Dimensions Area (m^2)	Depth (m)	Melt Mass M_f (kg)	Melt[a] Energy Q_m (MJ)	Melt Mass Averaged Particle Size (μm)	Conversion Ratio % η_{KE}	η_D	Comments
1B	16.0	0.37	0.61	14.0	39.2	242	1.1	2.6	First explosion
	12.0			18.7	52.4	242		5.1	η_{KE} not available
2B	6.0	0.37	0.30	18.6	52.0	2406	1.6	2.8	
3B	3.0	0.18	0.30	18.6	52.0	1174	1.3	4.0	
4B	12.0	0.37	0.61	18.7	52.4	332	1.3	5.7	Δ from ramp to plateau
						332	1.3	8.6	(Figure 5) Total ΔP
7B	1.5	0.18	0.15	12.0[b]	33.6	9012	0.3	0.2	
8B	15.0	0.37	0.76	18.7	52.4	162	1.5	5.9	Δ from ramp to plateau
							1.5	7.7	(Figure 5) Total ΔP
9B	9.0	0.37	0.46	18.7	52.4	1040	1.1	4.4	

[a] Based on 2.8 MJ/kg.

[b] Melt mass estimated from posttest debris. Only fragmented melt quantity used. Initial mass ratio based on 18.7 kg delivered.

They are also plotted against initial water/melt mass ratio in Figure 17 and in Figure 18 against water depth.

These figures show that the conversion ratio η_{KE} did not vary significantly with either mass ratio or water geometry with the exception of the extremely lean mass ratio (FITS7B). The values calculated from chamber pressure data for η_D show a dependence on these two parameters. Although the test matrix was rather sparse, this result suggests that as the water/melt mass ratio increased, the associated tamping increased the total utilization of the converted thermal energy. Then, since the kinetic energy held roughly constant, it would follow that the stored energy conversion ratio would increase.
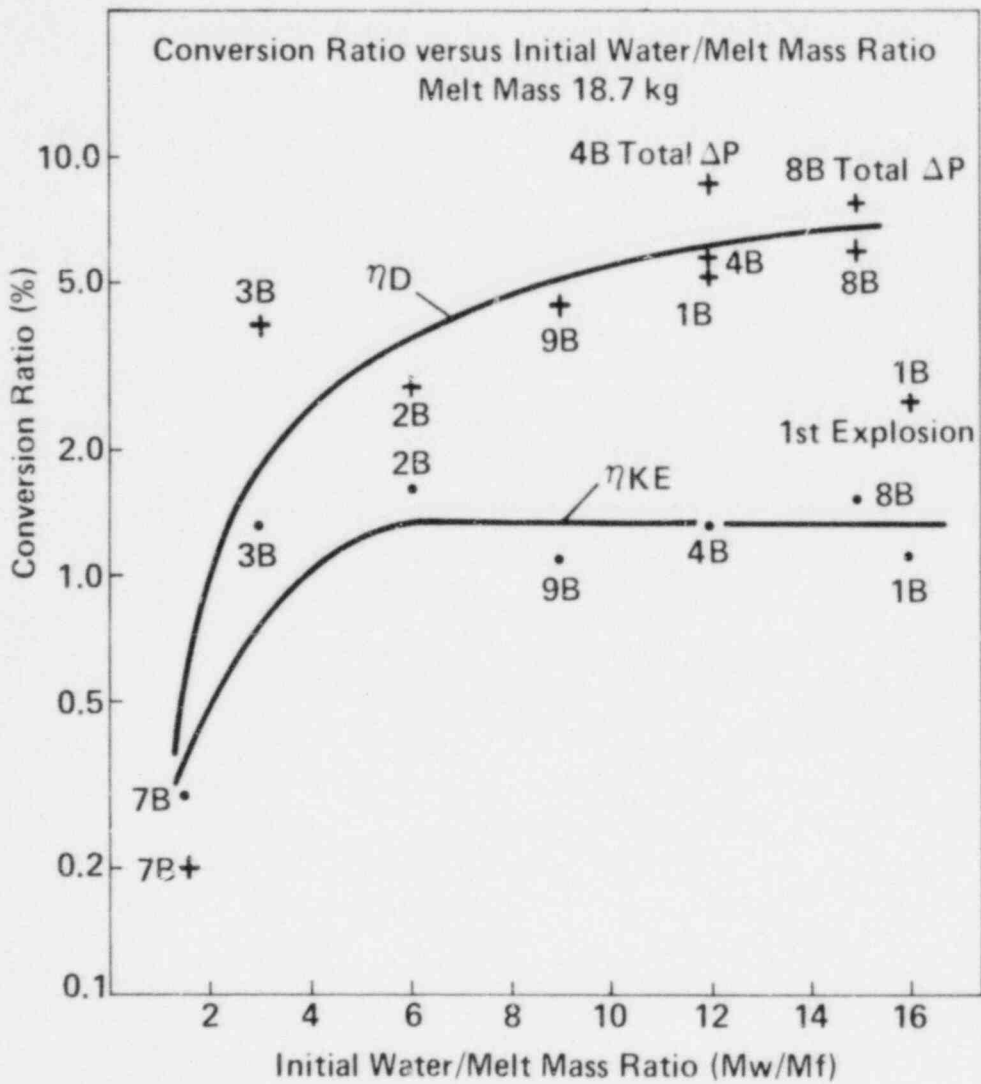
Figure 17. Conversion Ratio vs. Initial Water/Melt Mass Ratio, M_f = 18.7 kg
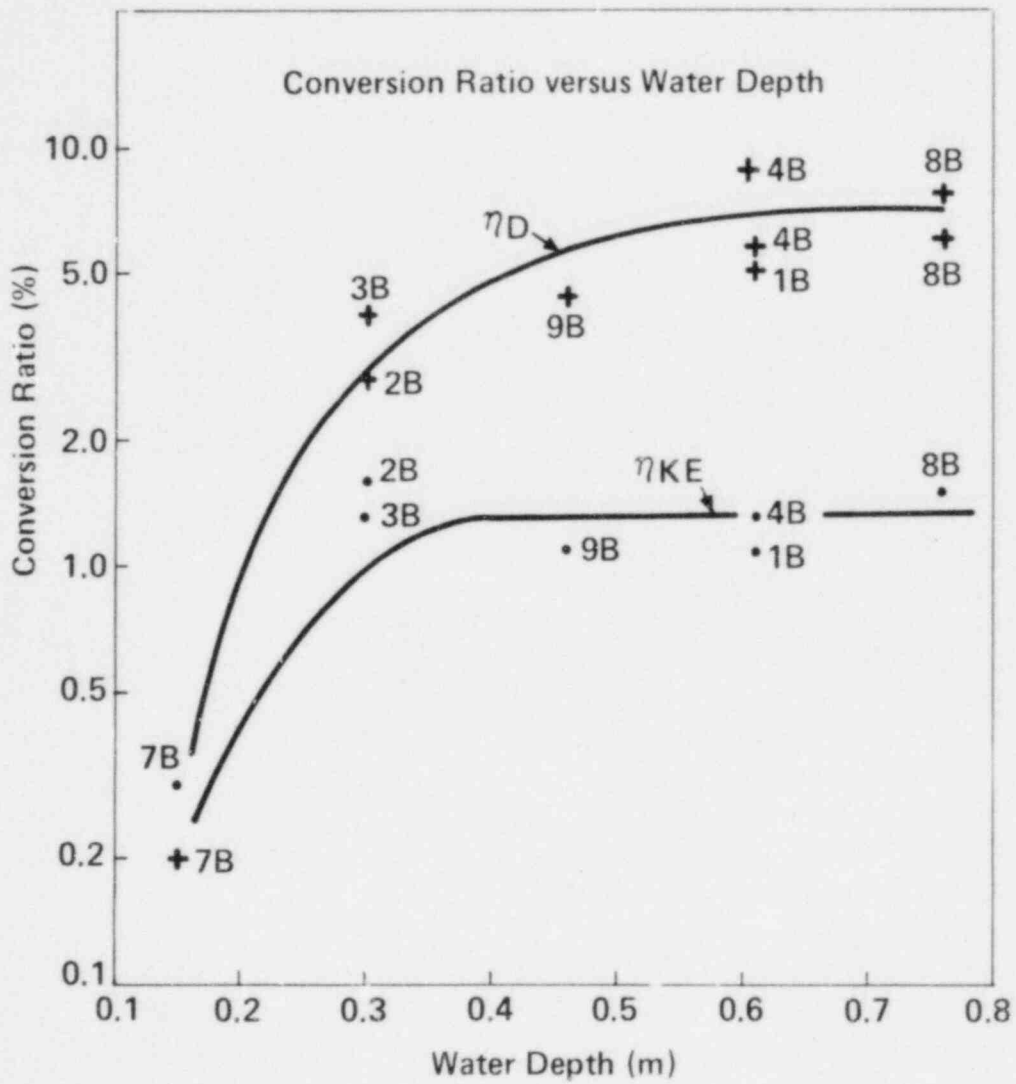
Figure 18. Conversion Ratio vs. Water Depth

5. DEBRIS CHARACTERISTICS

The sieved debris are characterized by the mass averaged particle size as shown in Table 2 and plotted versus total conversion ratio, η_{tot}, in Figure 19. This figure, together with Figures 17 and 18, show that mass ratio, water geometry, and debris size are related to the total converted energy of a given steam explosion; these aspects are under continuing investigation. Debris distributors for individual FITSB tests are included in Appendix B.
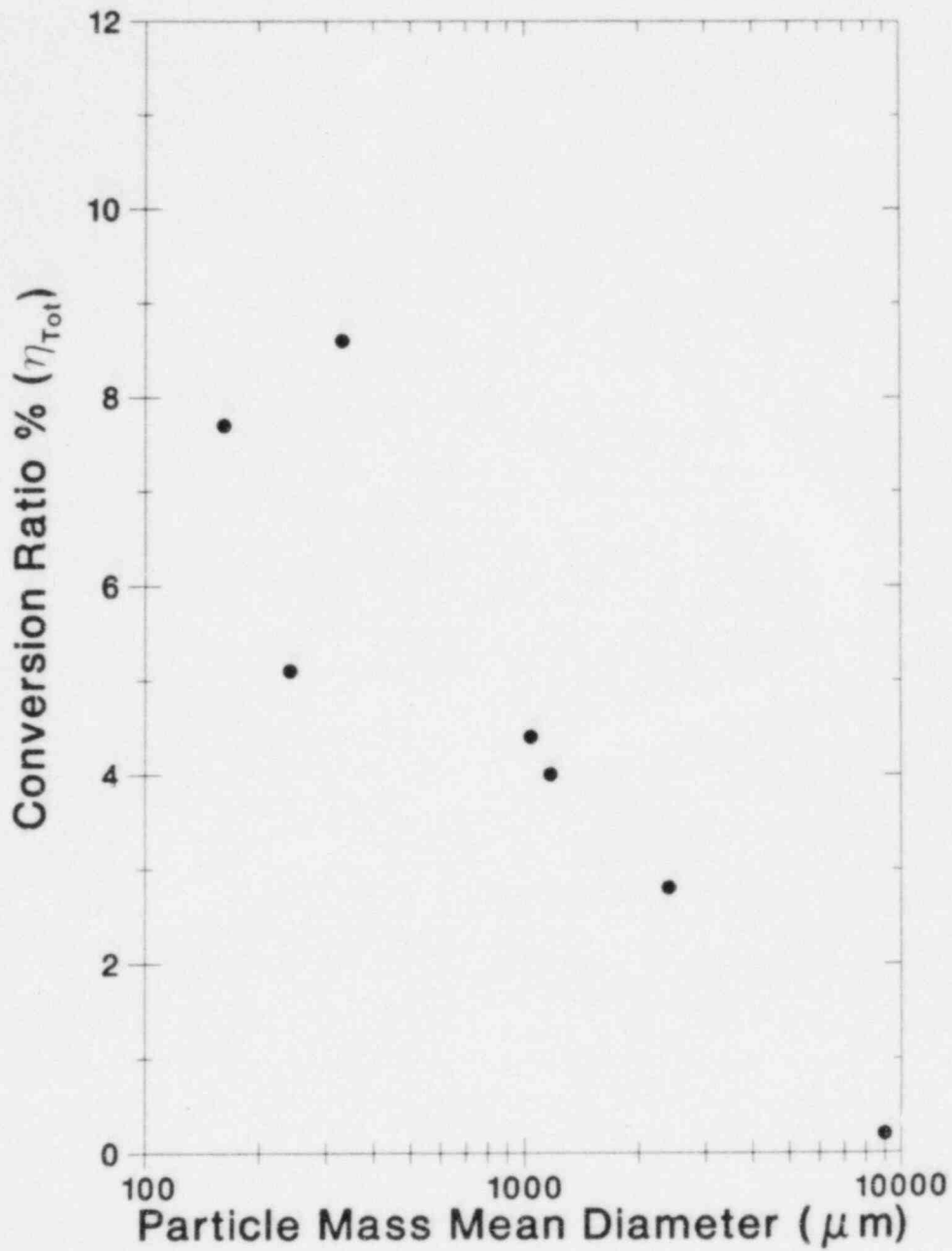
Figure 19. Total Conversion Ratio $\eta_{tot} = \eta_{KE} + \eta_D$ vs. Mass Average Particle Size From FITSB Posttest Debris

6. CONCLUSIONS

Under certain conditions, multiple explosions can occur in subcooled water, and a relatively weak explosion can provide energy to enhance coarse fragmentation in a larger melt mass. This enhanced fragmentation may either increase total steam explosion yield (more melt involved) or late-time pressurization due to steam generation.

Although not yet thoroughly understood in these experiments, water temperature is an important parameter. Spontaneous trigger sites observed in saturated water were not of sufficient strength to cause escalation into the propagation phase at this melt mass scale. There may be a melt mass threshold that depends on water temperature. The melt mass threshold for spontaneous explosions was found to be 1.8 kg for iron-alumina and 4 kg for corium A+R in 70° to 80°C subcooled water. In other aspects studied to date, the explosibility of corium A+R appears to be closely similar to iron-alumina. Steam explosion kinetic energy conversion ratio, η_{KE}, is relatively insensitive to initial mass ratio and depth and ranges from 0.3 percent to 2.6 percent over a mass ratio range of 1.5 to 57 when combining all the data for iron-alumina subcooled water tests.

The chamber pressurization conversion ratio, η_D, ranged over values from 1.8 percent to 8.6 percent and was sensitive as to whether a single or double explosion was involved. When considering the total utilization of transferred thermal energy from a melt, a value of $\eta_{tot} = \eta_{KE} + \eta_D = 9.9$ percent occurred with iron-alumina when producing a double explosion. Although now established as independent quantities, the rather large individual variations in η_{KE} and η_D might have been due to effects such as the following: some of the melt that did not participate in propagating steam explosion might have vaporized water in the early expansion phase; the amount of fuel that participated might have depended on the mass ratio, geometry, and type of explosion (single or multiple). As stated above, we are not implying that 9.9 percent of the available thermal energy represents the work fraction that would lead to missile generation or dynamic vessel failure in a hypothetical reactor accident. Rather, the 9.9 percent represents the maximum work available in a particular FITS experiment, deduced from chamber pressurization and material motion measurements. We emphasize that extrapolation of this result to a reactor accident requires a large amount of additional analyses; these analyses comprise a major task of the ongoing program at Sandia.

From a limited number of tests, an experimental investigation of the interaction of molten iron-alumina ($M_f = 18.7$ kg) with varying masses, M_c, of water produced the following results:

1. For a water subcooling of $\Delta T = 75°$ to $85°C$, the interaction was always explosive for $1.5 < M_c/M_f < 15$.

2. In particular, for $12 < M_c/M_f < 15$, the interaction produced two explosions separated by 120 to 140 ms.

3. For $3 < M_c/M_f < 15$, the kinetic energy conversion ratio was approximately constant at an average value $\eta_{KE} = 1.3$ percent.

4. The chamber stored energy conversion ratio, η_D, increased with M_c/M_f and reached values in the range of 5.1 percent to 8.6 percent when double explosions occurred.

5. With double explosions, it appeared that the first explosion enhanced coarse mixing for the second explosion.

6. For lower subcooling ($\Delta T \sim 1°C$) in one test, several trigger-like perturbations were observed, but none was strong enough to produce a propagating explosion.

REFERENCES

1. R. E. Henry, H. Hohmann, and H. Kottowski, "The Effect of Pressure on NaCl-H$_2$O Explosions," Fourth CNSI Specialist Meeting on Fuel-Coolant Interactions in Nuclear Reactor Safety, Bournemouth, United Kingdom, April 1979.

2. L. D. Buxton and W. B. Benedick, Steam Explosion Efficiency Studies, NUREG/CR-0947, SAND79-1399, Sandia National Laboratories, Albuquerque, NM, December 1979.

3. L. D. Buxton, W. B. Benedick, and M. L. Corradini, Steam Explosion Efficiency Studies: Part II--Corium Experiments, NUREG/CR-1746, SAND80-1324, Sandia National Laboratories, Albuquerque, NM, October 1980.

4. M. J. Bird, "Thermal Interactions Between Molten Uranium Dioxide and Water: An Experimental Study Using Thermite Generated Uranium Dioxide," ASME Winter Meeting on Fuel-Coolant Interactions HTD, Vol. 1, Washington, DC, November 15-20, 1981.

5. H. Kottowski, K. Mehr, and G. Grossi, "Vapor Explosion Studies in a Constrained Geometry and Forced Fragmentation and Mixing," ASME Winter Meeting on Fuel-Coolant Interactions HTD, Vol. 1, Washington, DC, November 15-20, 1981.

6. M. L. Corradini, Analysis and Modeling of Steam Explosion Experiments, NUREG/CR-2131, SAND80-2072, Sandia National Laboratories, Albuquerque, NM, April 1981.

7. M. L. Corradini and D. V. Swenson, Probability of Containment Failure Due to a Steam Explosion Following A Postulated Core Meltdown in an LWR, NUREG/CR-2214, SAND80-2132, Sandia National Laboratories, Albuquerque, NM, June 1981.

8. M. Berman, Light Water Reactor Safety Research Program Semiannual Report, October 1981-March 1982, NUREG/CR-2841, SAND82-1572, December 1982.

9. D. E. Mitchell, M. L. Corradini, and W. W. Tarbell, Intermediate Scale Steam Explosion Phenomena: Experiments and Analyses, NUREG/CR-2145, SAND81-0124, Sandia National Laboratories, Albuquerque, NM, September 1981.

10. M. L. Corradini, D. E. Mitchell, and L. S. Nelson, "Recent Experiments and Analyses Regarding Steam Explosions with Simulant Molten Reactor Fuels," ASME Winter Meeting on Fuel-Coolant Interactions, HTD, Vol. 1, Washington, DC, November 15-20, 1981.

APPENDIX A

Melt Control Sequence (Figure A1)

At time $t = 0$, the program ARTISAN turns on the ignition voltage that heats the ignitor and starts the thermite burn. As the burn proceeds, sensors I_1, I_2, and I_3 are bridged, which sends signals to the burn-rate conditioner. The output of the burn rate conditioner sends a signal to the signal mixer and then to the visicorder for burn-rate data. The I_3 signal also goes to the camera start either time-delayed or direct, and time-delayed to the cylinder relay for the cylinder drop. When the melt reaches melt-sensor MS1 or MS2, a signal is sent to the melt sensor conditioner. The output of the melt sensor conditioner sends the MS1 and MS2 signals to the signal mixer and then to the visicorder. Also, MS1 and MS2 signals are paralleled and time-delayed into the capacitor discharge unit, which fires the detonator. MS1 and MS2 are locked out to prevent them from sensing any vented melt until cylinder drop has occurred and an approximate time allowance has been made for the free full distance to the coolant surface.
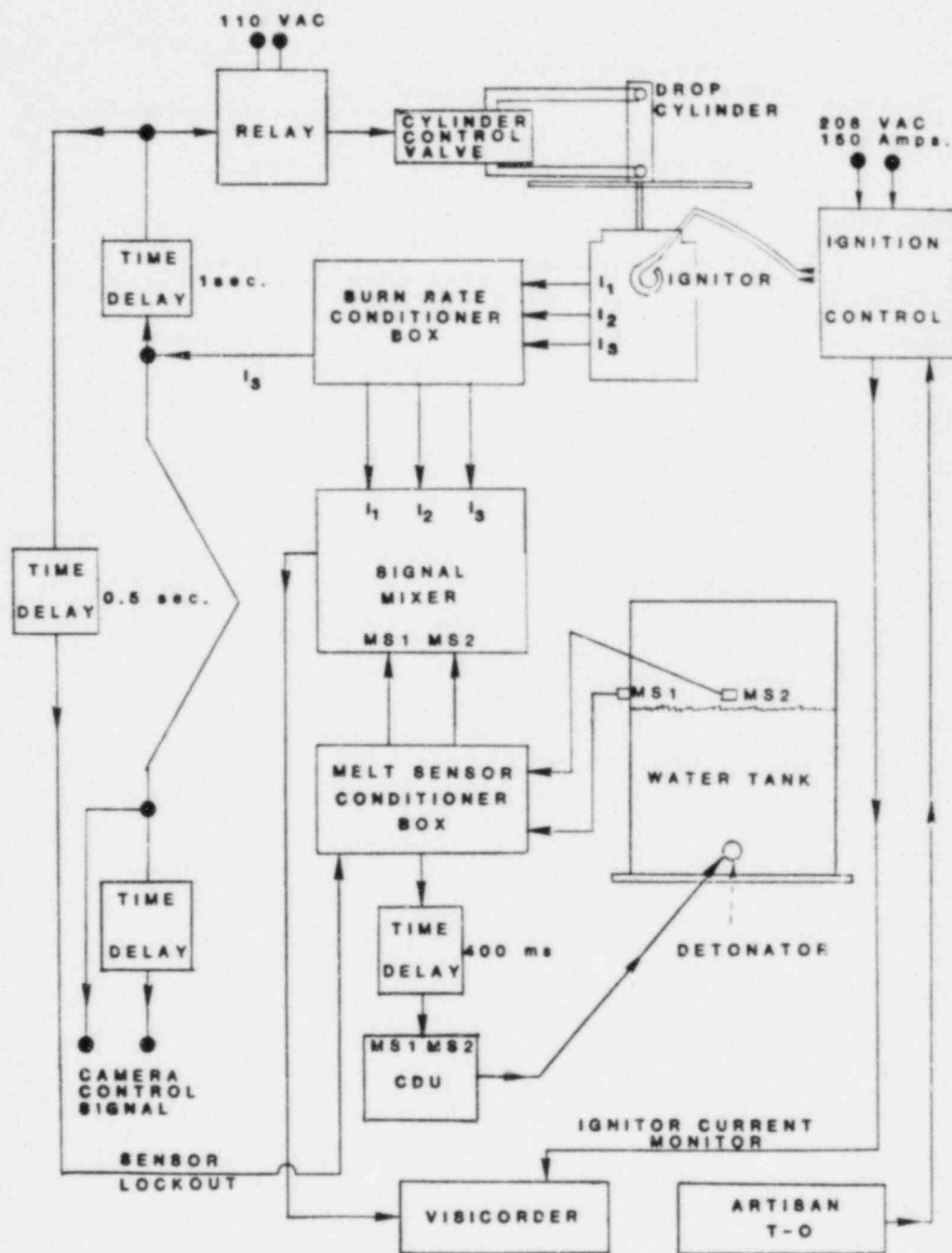
Figure A1. Melt Control Sequence

APPENDIX B

Debris Distribution Data

For purposes of reference, the histograms from sieving the debris from the FITSB tests are shown in Figures B1 through B8. Figures B9, B10, and B11 show the cumulative debris size distributions from tests involving double explosions, single explosions, and weak or nonexplosive interactions, respectively. These results were used for calculating the mass-averaged particle sizes that were plotted against total energy conversion ratio in Figure 19.
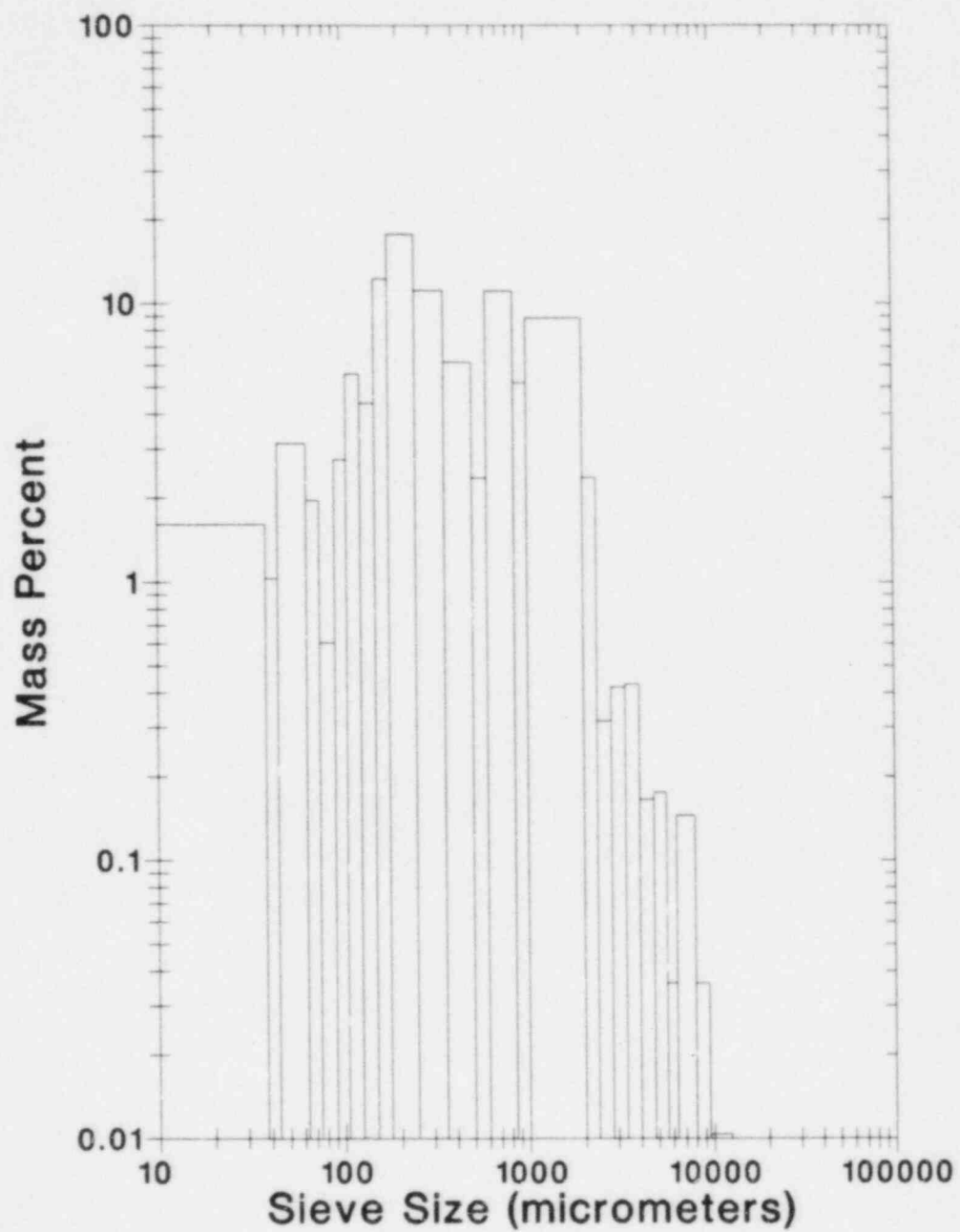
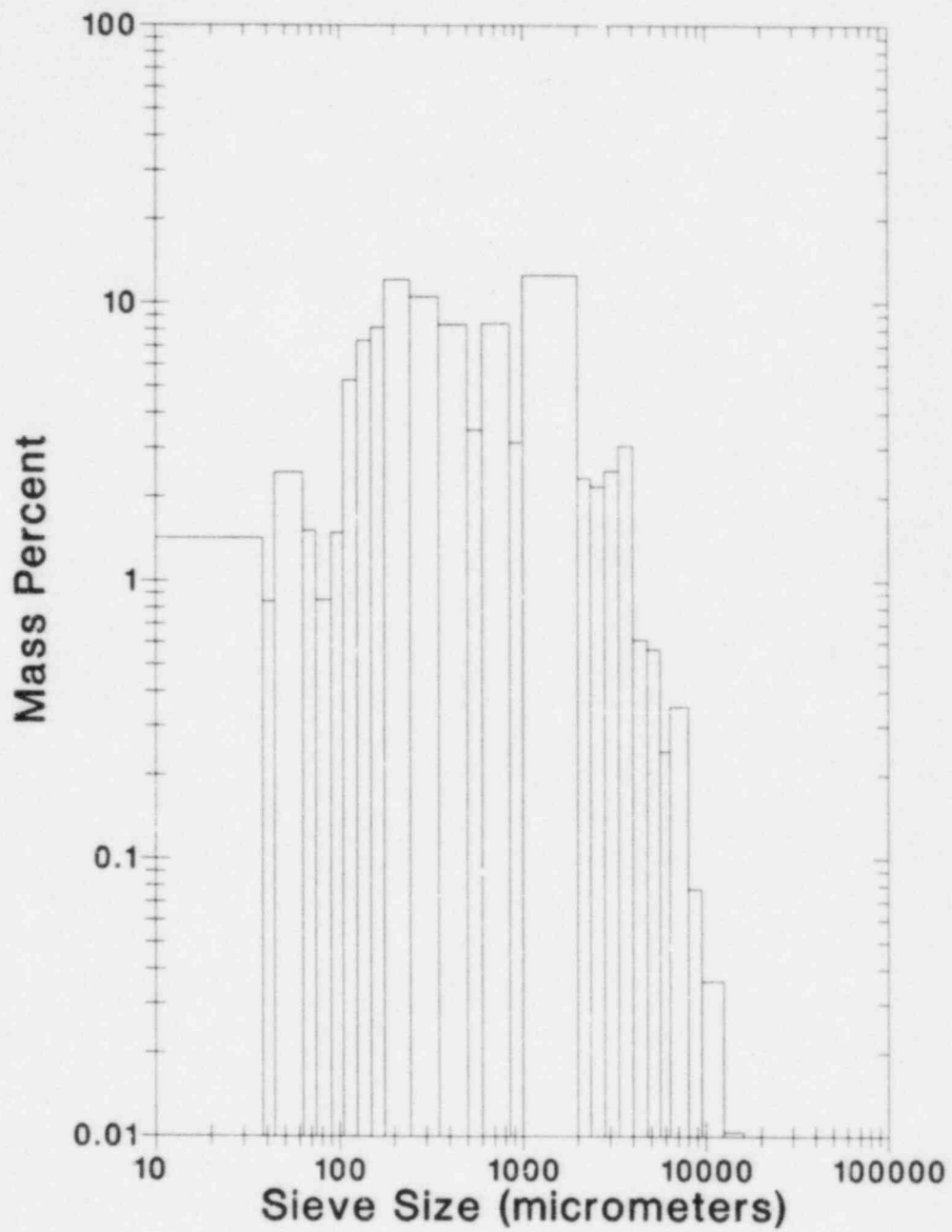Figure B1. FITS1B Particle Size Distribution $M_W/M_f = 12$

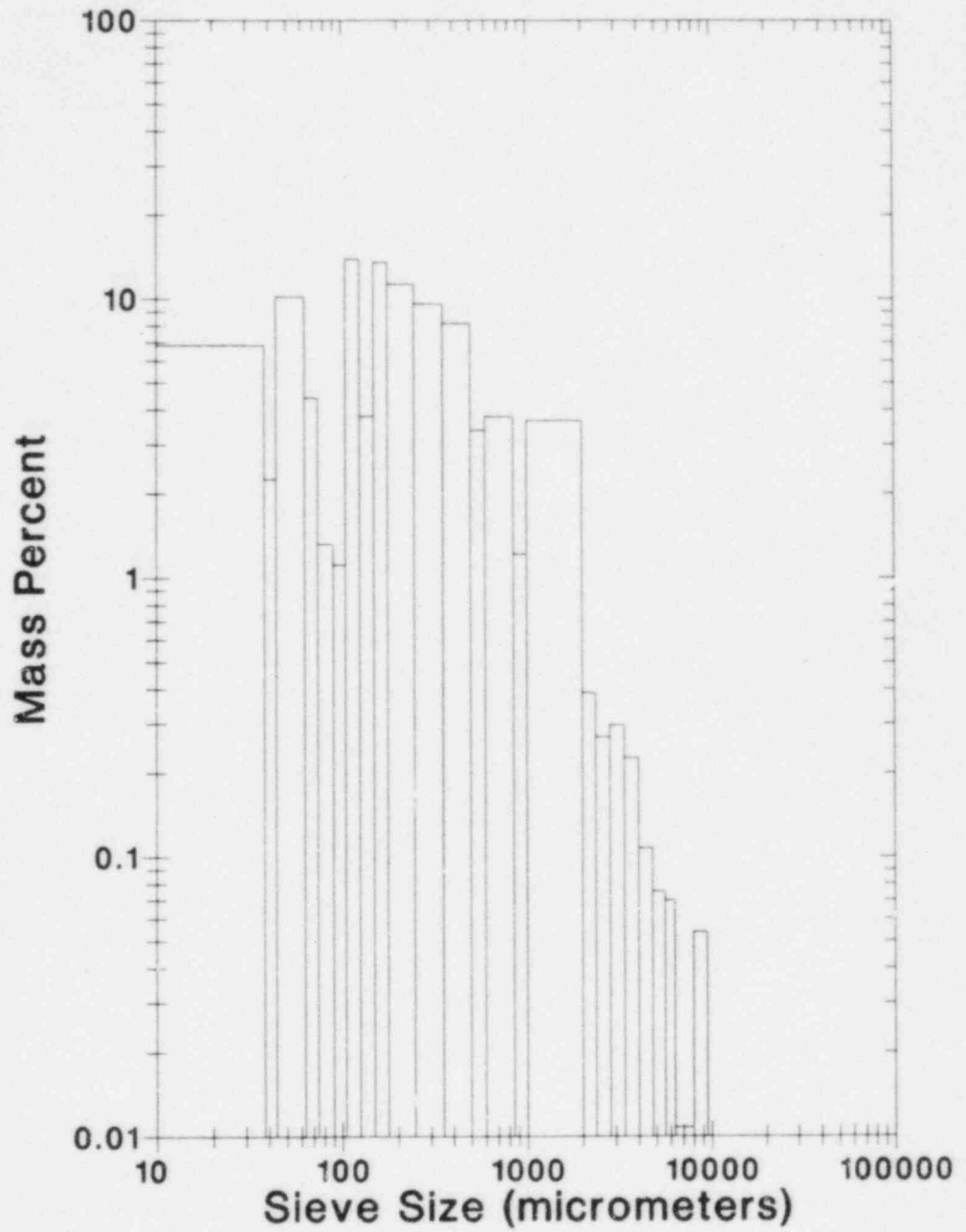Figure B2. FITS4B Particle Size Distribution M_W/M_f = 12

Figure B3. FITS8B Particle Size Distribution. Double
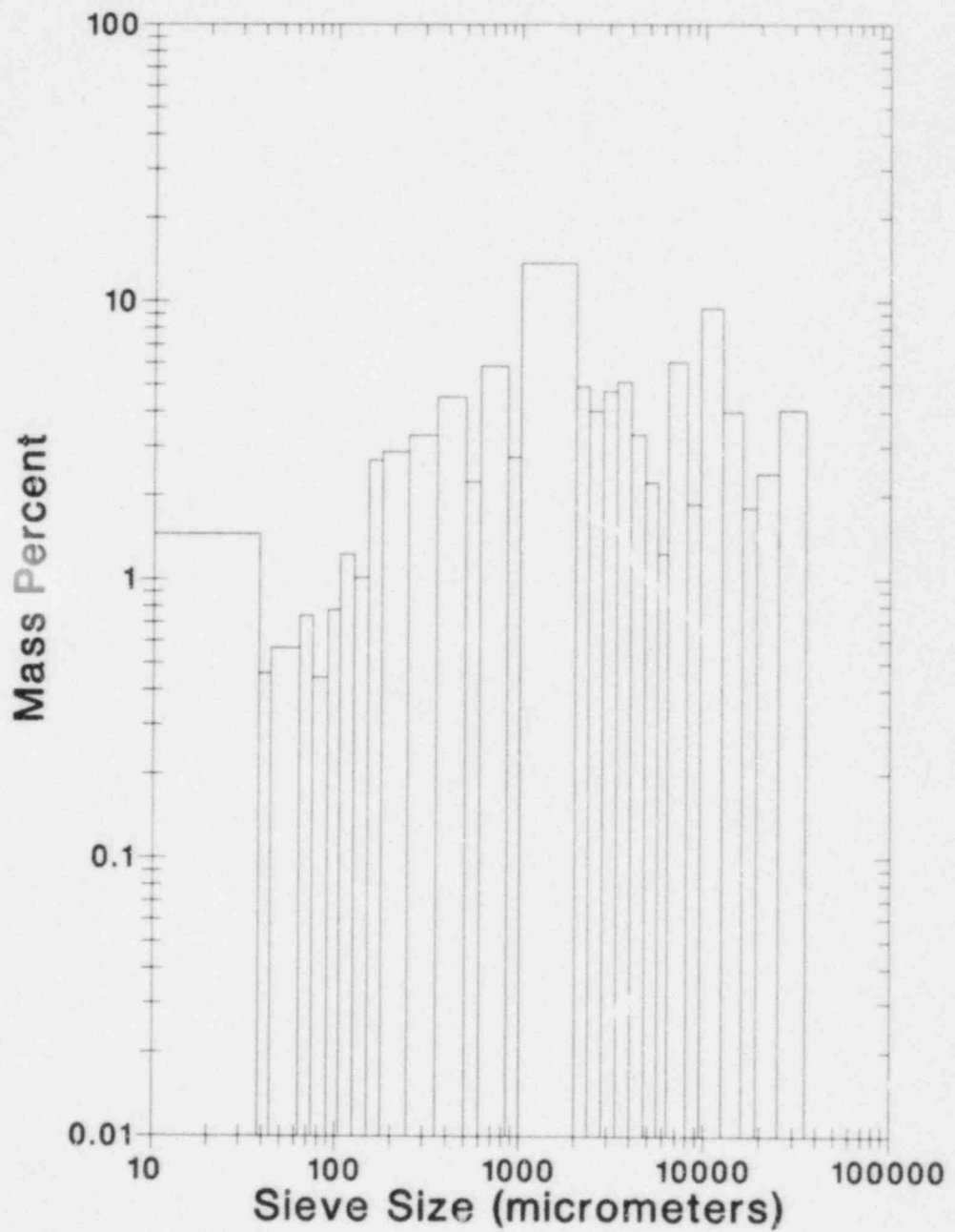explosion. $M_W/M_f = 15$.

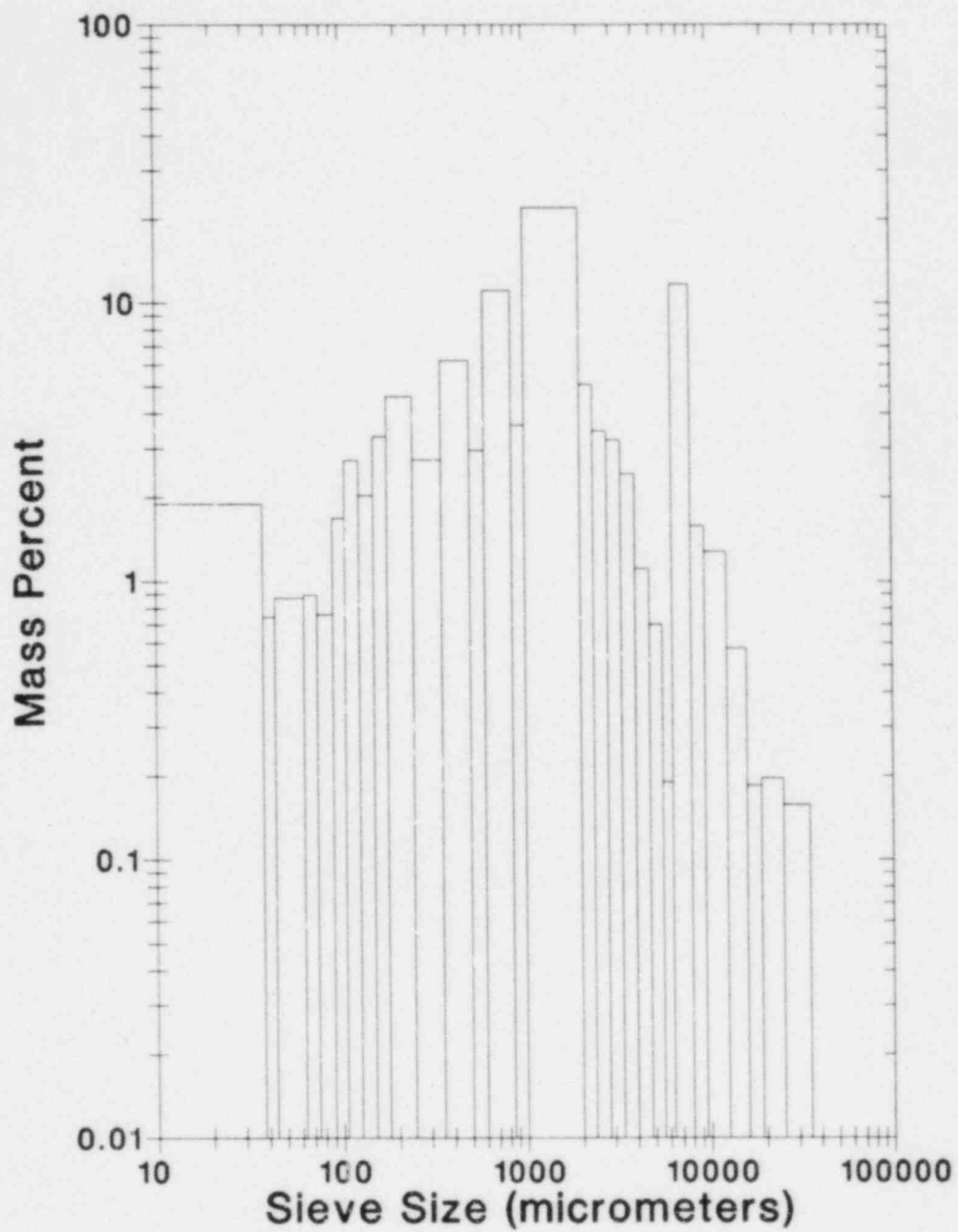Figure B4. FITS2B Particle Size Distribution $M_w/M_f = 6$

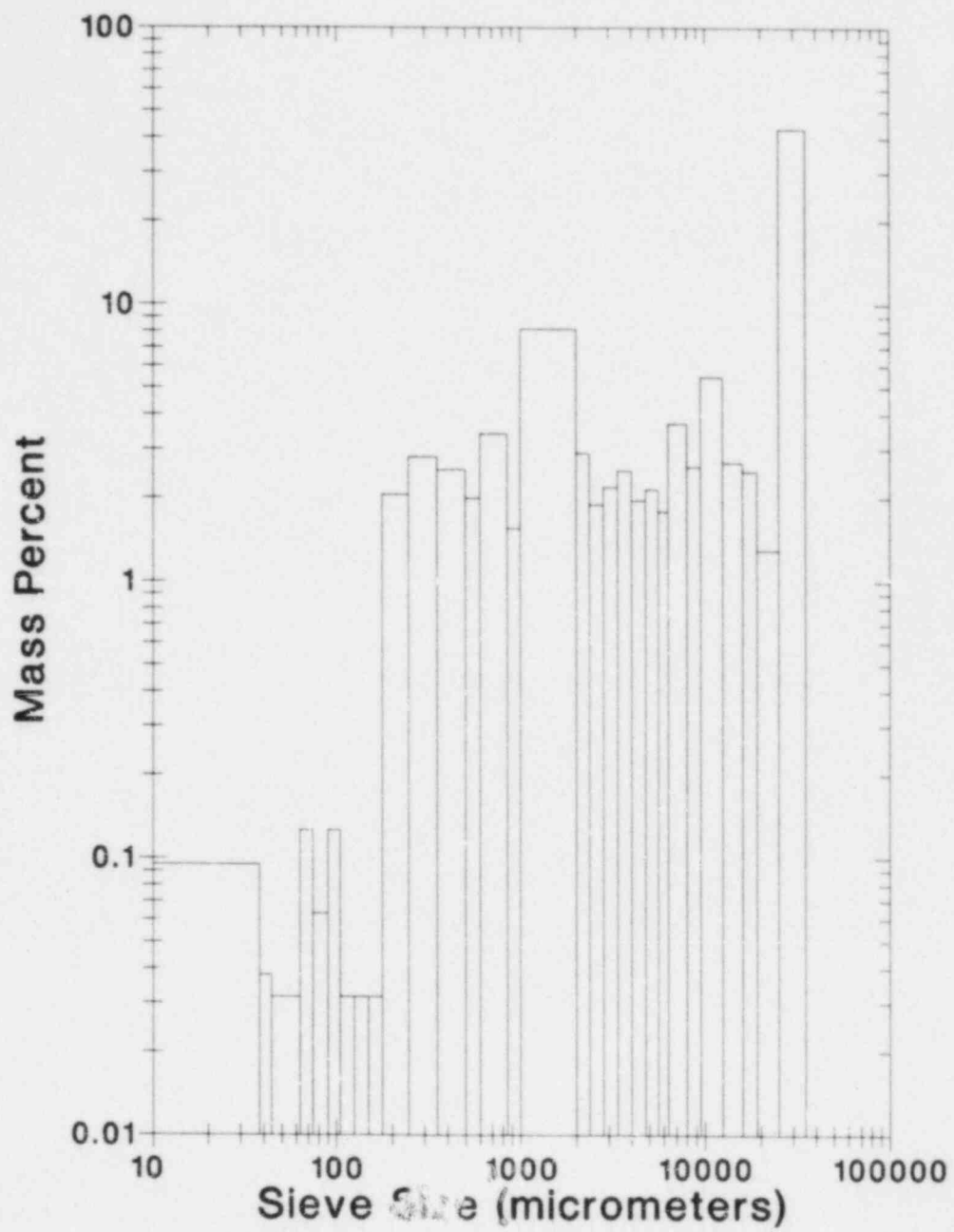Figure B5. FITS3B Particle Size Distribution $M_W/M_f = 3$

Figure B6.   FITS6B Particle Size Distribution M_w/M_f = 3.4. Saturated Water.
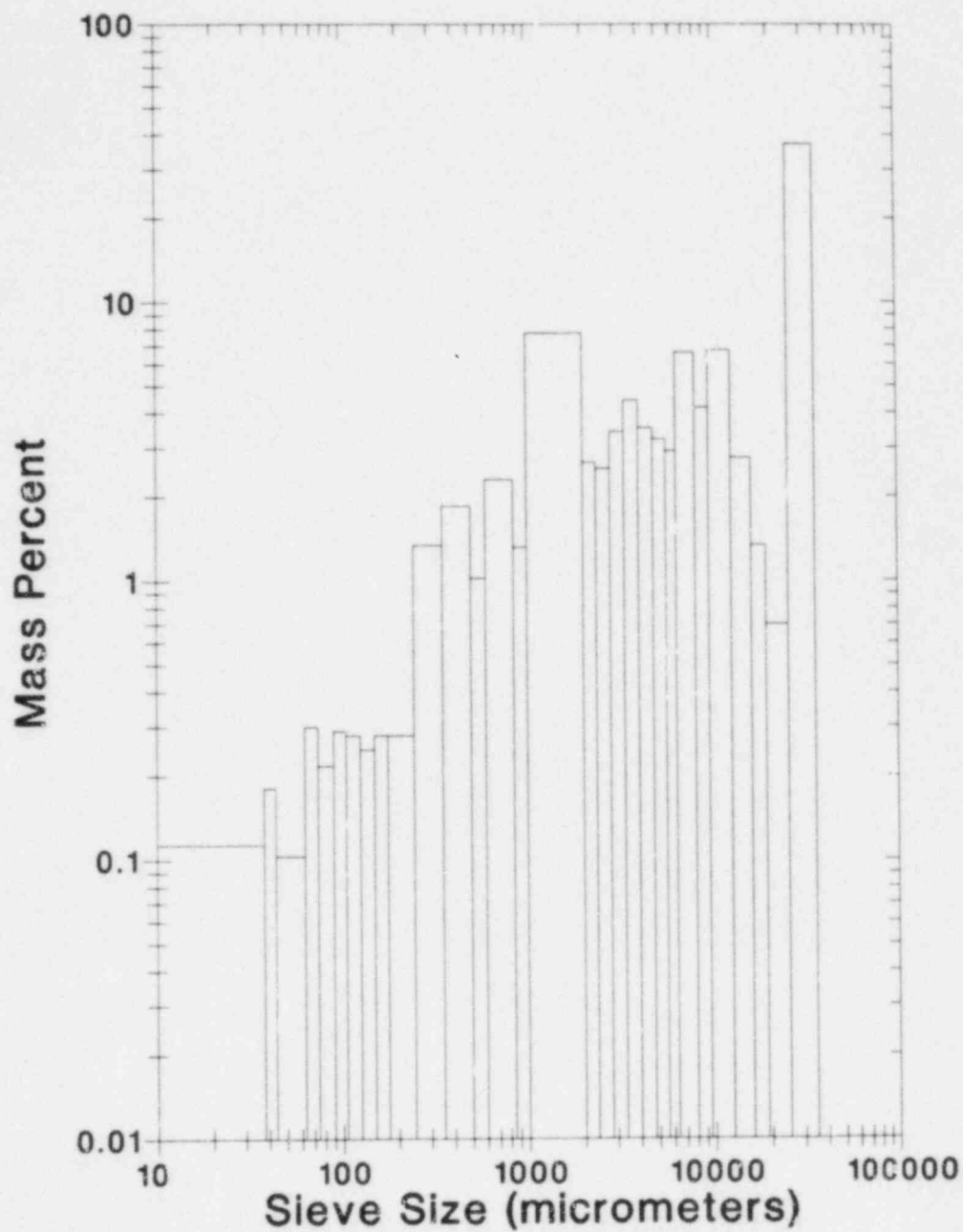
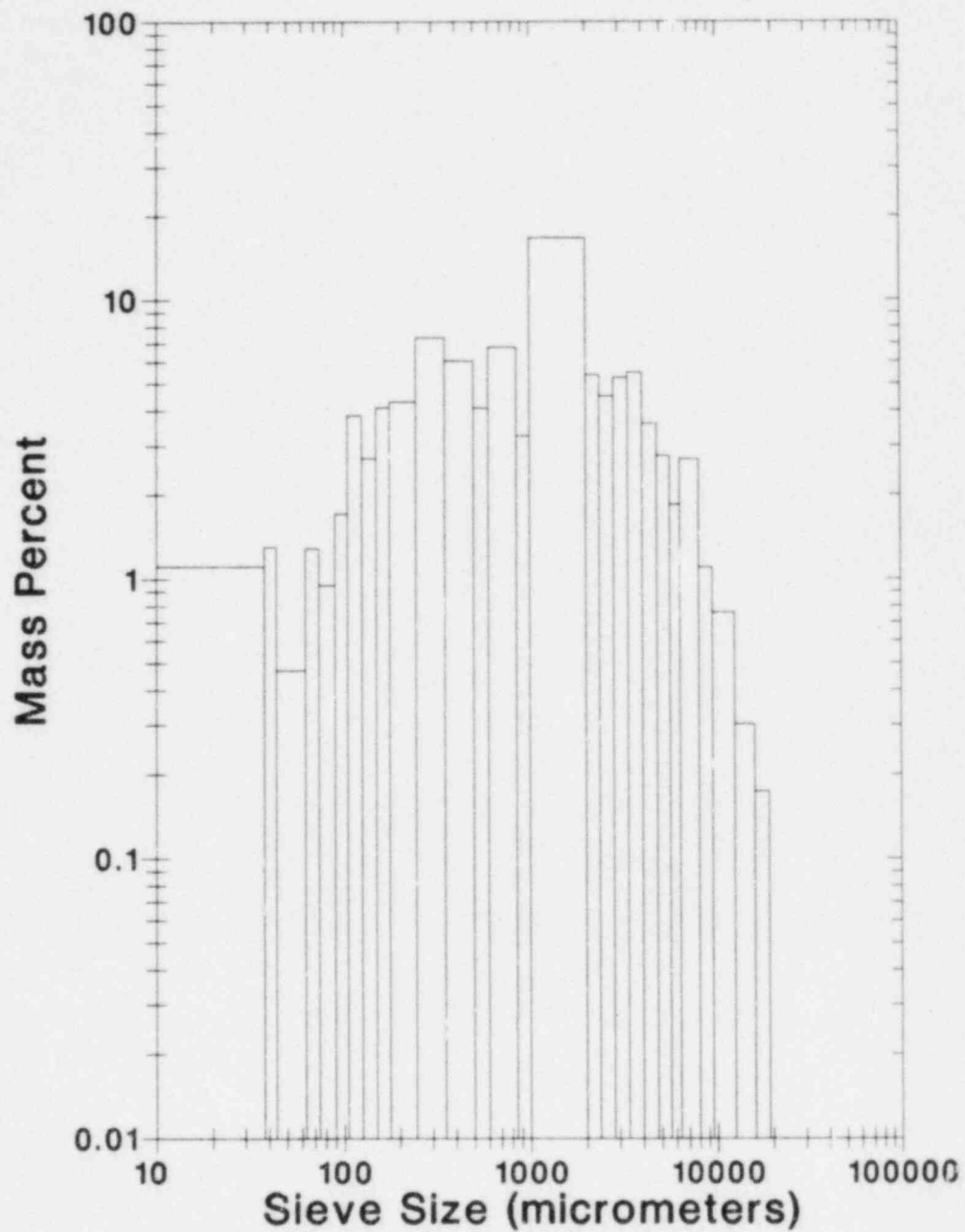Figure B7. FITS7B Particle Size Distribution $M_w/M_f = 1.5$

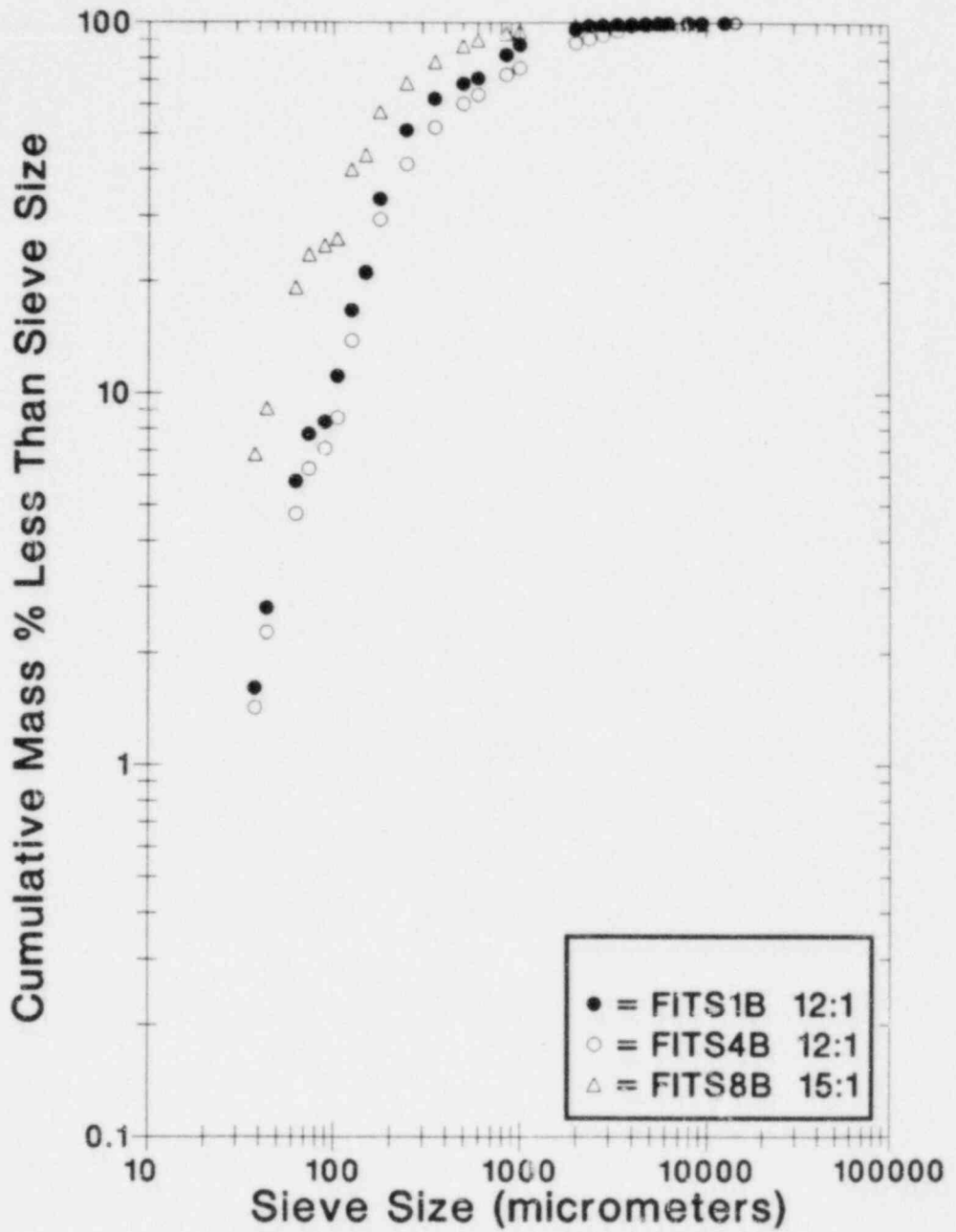Figure B8. FITS9B Particle Size Distribution M_w/M_f = 9

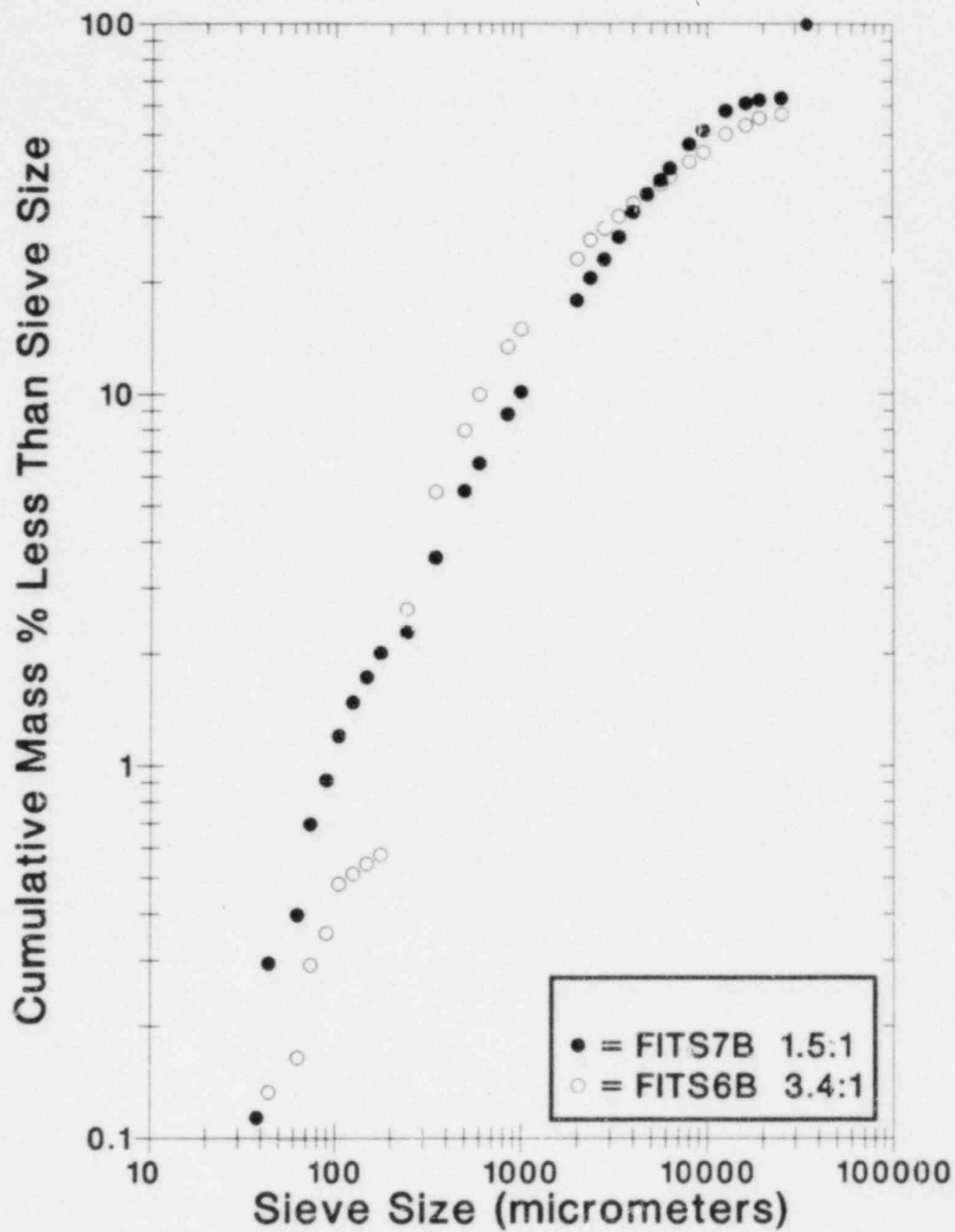Figure B9. Cumulative Debris Size Distributions

Figure B10. Cumulative Debris Size Distributions
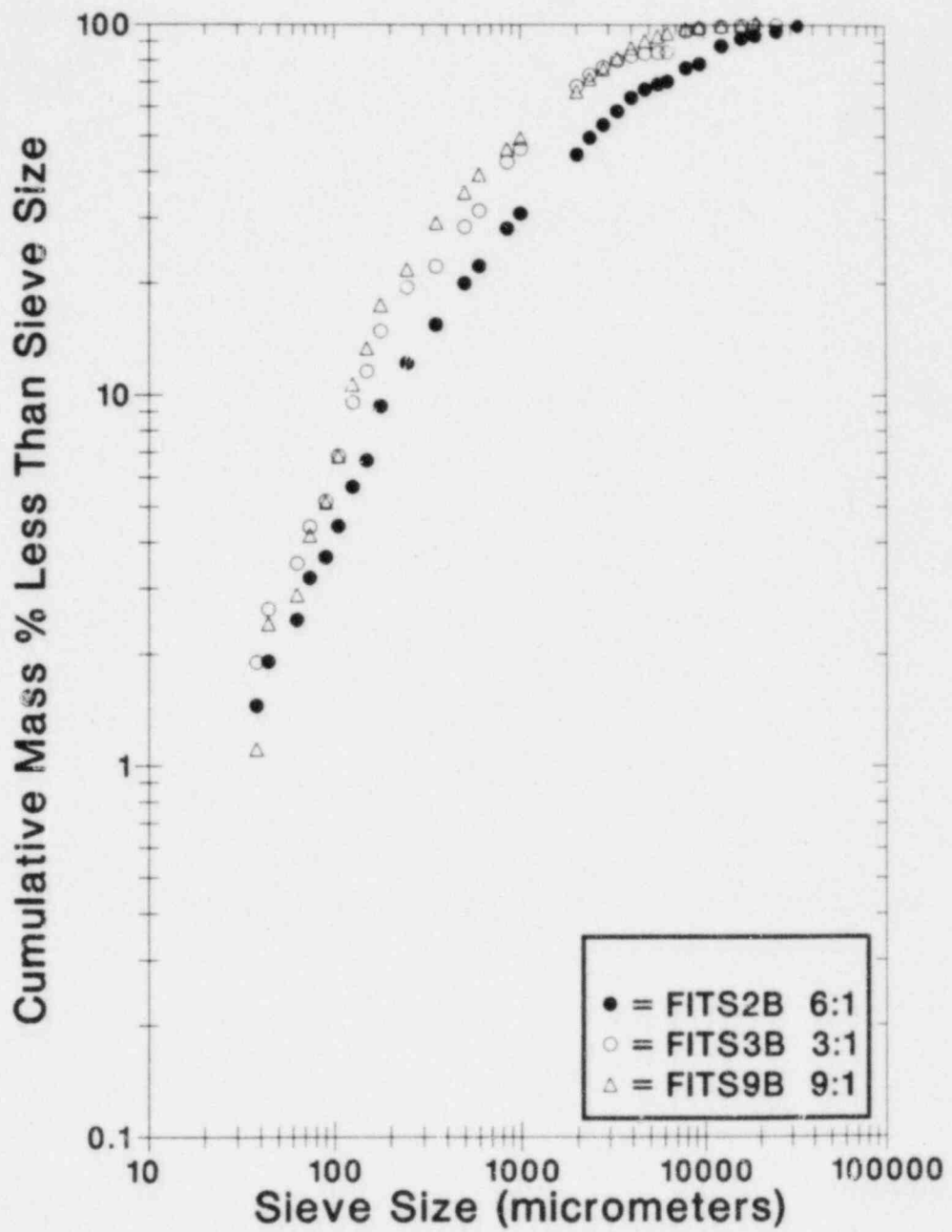
Figure B11. Cumulative Debris Size Distributions

Distribution:
U.S. Government Printing Office
Receiving Branch (Attn: NRC Stock)
8610 Cherry Lane
Laurel, MD 20707
275 copies for R3

U. S. Nuclear Regulatory Commission   (6)
Office of Nuclear Regulatory Research
Washington, DC 20555
Attn: R. T. Curtis
       J. Hopenfeld
       C. N. Kelber
       D. F. Ross
       P. Worthington
       N. Zuber

U. S. Nuclear Regulatory Commission   (5)
Office of Nuclear Regulatory Research
Washington, DC 20555
Attn: S. B. Burson
       M. Silberberg
       J. L. Telford
       T. J. Walker
       R. W. Wright

U. S. Nuclear Regulatory Commission   (3)
Office of Nuclear Reactor Regulation
Washington, DC 20555
Attn: C. Allen
       J. Rosenthal
       Z. Rosztoczy

Applied Sciences Association, Inc.
P. 0. Box 2687
Palos Verdes Pen., CA 90274
Attn: D. Swanson

Argonne National Laboratory   (4)
9700 South Cass Avenue
Argonne, IL 60439
Attn: R. P. Anderson
       D. Armstrong
       Dae Cho
       B. Spencer

Battelle Columbus Laboratory (2)
505 King Avenue
Columbus, OH 43201
Attn: P. Cybulskis
R. Denning

Brookhaven National Laboratory (4)
Upton, NY 11973
Attn: R. A. Bari
T. Ginsberg
G. A. Greene
T. Pratt

Cornell University
School of Civil and Environmental
Engineering
Hollister Hall
Ithaca, NY 14853
Attn: D. V. Swenson

EG&G Idaho (2)
Willow Creek Building, W-3
P. O. Box 1625
Idaho Falls, ID 83415
Attn: Richard Moore
Server Sadik

Electric Power Research Institute (3)
3412 Hillview Avenue
Palo Alto, CA 94303
Attn: J. J. Haugh
G. Thomas
R. Vogel

Fauske & Associates (2)
627 Executive Drive
Willowbrook, IL 60521
Attn: H. Fauske
R. Henry

Los Alamos National Laboratory (4)
P. O. Box 1663
Los Alamos, NM 87545
Attn: C. Bell
W. R. Bohl
R. G. McQueen
K. H. Wohletz

Northwestern University
Chemical Engineering Department
Evanston, IL 60201
Attn: S. G. Bankoff

NUS Corporation   (2)
4 Research Place
Rockville, MD 20850
Attn: G. W. Parry
      R. Sherry

Sandia National Laboratories
Division 6427
P. O. Box 5800
Albuquerque, NM 87185
Attn: G. Shaw   (20)

TVA
400 Commerce Avenue
W56178C-K
Knoxville, TN 37902
Attn: Dave Simpson

UCLA
Nuclear Energy Laboratory
405 Hilgard Avenue
Los Angeles, CA 90024
Attn: I. Catton

University of California at
  Santa Barbara
Chemical and Nuclear Eng. Dept.
Santa Barbara, CA 93106
Attn: T. G. Theofanous

University of Virginia
Dept. of Nuclear Engineering and
  Engineering Physics
Thornton Hall
Charlottesville, VA 22904
Attn: Dr. Albert B. Reynolds

Westinghouse Corporation
Nuclear Energy Systems
P.O. Box 350
Pittsburgh, PA 15230
Attn: Larry E. Hochreiter

University of Wisconsin   (3)
Nuclear Engineering Department
1500 Johnson Drive
Madison, WI   53706
Attn: M. L. Corradini

CEC
Director of Research, Science & Education
Rue De La Loi 200
1049 Brussels
BELGIUM
Attn: B. Tolley

McGill University   (2)
315 Querbes
Outremont, Quebec
CANADA H2V 3W1
Attn: John H. S. Lee

Battelle Institut E. V.   (2)
Am Roemerhof 35
6000 Frankfurt am Main 90
FEDERAL REPUBLIC OF GERMANY
Attn: Dr. Werner Baukal
        Dr. G. Langer

Institute für Kernenergetik
    und Energiesysteme   (3)
University of Stuttgart
Pfaffenwaldring 31
Postfach 801140
D-7000 Stuttgart 80 (Vaihingen)
FEDERAL REPUBLIC OF GERMANY
Attn: M. Buerger
        G. Froehlich
        H. Unger

Kernforschungszentrum Karlsruhe   (2)
Postfach 3640
D-7500 Karlsruhe 1
FEDERAL REPUBLIC OF GERMANY
Attn: H. Jacobs
        H. Rininsland

Kernforschungszentrum Karlsruhe   (2)
Postfach 3640
75 Karlsruhe
FEDERAL REPUBLIC OF GERMANY
Attn: Dr. J. P. Hosemann
        Dr. M. Reimann

Kraftwerk Union
Hammerbacherstrasse 12 & 14
Postfach 3220
D-8520 Erlangen 2
FEDERAL REPUBLIC OF GERMANY
Attn: Dr. M. Peehs

Technische Universitaet Hannover
3000 Hannover 1
FEDERAL REPUBLIC OF GERMANY
Attn: Prof. F. Mayinger

Technische Universitaet Muenchen
D-8046 Garching
FEDERAL REPUBLIC OF GERMANY
Attn: Dr. H. Karwat

Commissariat a l'Energie Atomique
Centre d'Etudes Nucleaires
    de Fontenay-aux-Roses
(IPSN)
Boite Postale 6
F-92260 Fontenay-aux-Roses
FRANCE
Attn: Jacques Pelce

Commissariat a l'Energie Atomique
Centre d'Etudes Nucleaires de Grenoble
B.P. No. 85 X - Centre de Tri
F-38041 Grenoble Cedex
FRANCE
Attn: M. Georges Berthoud

DECPU/SEFCA
C.E.N. Cadarache
BP No. 1
13115 Saint-Paul LEZ-Durance
FRANCE
Attn: Patrick Herter

OECD Nuclear Energy Agency
38 Boulevard Suchet
F-75016 Paris
FRANCE
Attn: Dr. Jacques Royen

CNEN NUCLIT
Dipartimento Reattori Veloci
S. P. Anguillarese km 1+3400
C.P. No. 2400, I-001000
Rome
ITALY
Attn: Giovanni Scarano

ENEA
Nucleare e della Protezione Sanitaria (DISP)
Viale Regina Margherita, 125
Casella Postale N. 2358, I-00100
Rome
ITALY
Attn: Carlo Zaffiro

Euratom-Joint Research Centre
Ispra Establishment
Commission of the European Communities
C. P. No. 1, I-21020 Ispra (Varese)
ITALY
Attn: Dr. Ing. Heinz Kottowski

Euratom-Joint Research Centre
Ispra Establishment
Commission of the European Communities
C. P. No. 1, I-21027 Ispra (Varese)
ITALY
Attn: Mrs. Paola Fasoli-Stella

FBR Safety Laboratory
Oarai Engineering Center
P.N.C.
Oarai-Machi, Higashi
Ibaraki-Gun, Ibarake-ken
JAPAN
Attn: Katsuro Takahashi

Japan Atomic Energy Research Institute
Tokai Establishment
Takai-mura, Naka-gun
Ibaraki-ken 319-11
JAPAN
Attn: Dr. Kazuo Sato

Swedish Nuclear Power Inspectorate
Statens Karnkraftinspektion
P.O. Box 27106
S-102, 52 Stockholm
SWEDEN
Attn: Lars G. Hobgerg

Swedish State Power Board
El-Och Vaermeteknik
SWEDEN
Attn: Eric Ahlstroem

AERE Harwell
Didcot
Oxfordshire OX11 ORA
UNITED KINGDOM
Attn: J. R. Matthews, TPD

University of Aston in Birmingham   (2)
Department of Chemistry
Gosta Green, Birmingham B47ET
UNITED KINGDOM
Attn: A. T. Chamberlain
       F. M. Page

Berkeley Nuclear Laboratory   (3)
Berkeley GL 139PB
Gloucestershire
UNITED KINGDOM
Attn: J. E. Antill
       S. J. Board
       N. Buttery

British Nuclear Fuels, Ltd
Building 396
Springfield Works
Salwick, Preston
Lancs
UNITED KINGDOM
Attn: W. G. Cunliffe

H. M. Nuclear Installations Inspectorate   (2)
Thames House North
Millbank, London SW1
UNITED KINGDOM
Attn: R. D. Anthony
        S. A. Harbison

University of Loughborough
Department of Physics
Loughborough
UNITED KINGDOM
Attn: J. Sturgess

National Nuclear Corp. Ltd.   (2)
Cambridge Road
Whetestone, Leicester, LE83LH
UNITED KINGDOM
Attn: F. P. O. Ashworth
        R. May

Simon Engineering Laboratory   (2)
University of Manchester
M139PL
UNITED KINGDOM
Attn: Prof. W. B. Hall
        S. Garnett

UKAEA Culham Laboratories   (3)
Abingdon, Oxon OX143DB
UNITED KINGDOM
Attn: F. Briscoe
        I. Cook
        B. D. Turland

UKAEA Safety & Reliability Directorate   (6)
Wigshaw Lane, Culcheth
Warrington WA34NE
Cheshire
UNITED KINGDOM
Attn: F. R. Allen
        J. H. Gittus
        A. N. Hall
        M. R. Hayns
        K. McFarlane
        R. S. Peckover

```
UKAEA AEE Winfrith                      (4)
Dorchester
Dorset DT2 8DH
UNITED KINGDOM
Attn:  M. Bird
       A. J. Briggs
       D. Fletcher
       R. Potter
       A. J. Wickett


Sandia Distribution:
1652   N. A. Evans  (5)
2513   D. E. Mitchell  (5)
6400   A. W. Snyder
6410   J. W. Hickman
6411   V. L. Behr
6411   A. S. Benjamin
6411   A. L. Camp
6415   F. E. Haskin
6415   J. M. Griesmeyer
6420   J. V. Walker
6421   P. S. Pickard
6422   D. A. Powers
6423   T. R. Schmidt
6425   W. J. Camp
6425   W. Frid
6425   M. Pilch
6425   S. D. Unwin
6425   M. F. Young
6427   M. Berman  (5)
6427   J. T. Hitchcock
6427   B. W. Marshall, Jr.
6427   L. S. Nelson
6427   0. P. Seebold
6427   M. P. Sherman
6427   D. W. Stamps
6427   S. R. Tieszen
6427   C. C. Wong
6440   D. A. Dahlgren
6442   W. A. von Riesemann
6444   L. D. Buxton
6449   K. D. Bergeron
8024   P. W. Dean
3141   S. A. Landenberger  (5)
3151   W. L. Garner
```

2 TITLE AND SUBTITLE	3 LEAVE BLANK	
STEAM EXPLOSION EXPERIMENTS AT INTERMEDIATE SCALE: FITSB SERIES		
	4 DATE REPORT COMPLETED	
	MONTH	YEAR
5 AUTHOR(S)		
D. E. Mitchell and N. A. Evans	6 DATE REPORT ISSUED	
	MONTH	YEAR
7 PERFORMING ORGANIZATION NAME AND MAILING ADDRESS (Include Zip Code)	8 PROJECT/TASK/WORK UNIT NUMBER	
Sandia National Laboratories Albuquerque, NM 87185	9 FIN OR GRANT NUMBER	
	A1030	
10 SPONSORING ORGANIZATION NAME AND MAILING ADDRESS (Include Zip Code)	11a TYPE OF REPORT	
Division of Accident Evaluation Office of Nuclear Regulatory Research U.S. Nuclear Regulatory Commission Washington, DC 20555	topical	
	b PERIOD COVERED (Inclusive dates)	
12 SUPPLEMENTARY NOTES		

13 ABSTRACT (200 words or less)

Experiments in the FITS chamber have been performed in which 18.7 kg of molten iron-alumina core melt simulant was delivered into water chambers in which the water mass was 1.5 to 15 times greater than the melt. Experiments in subcooled water showed that spontaneous explosions occurred over the range of water/melt mass ratio and geometry used and that in certain experiments, double explosions occurred. With double explosions, the first explosion enhanced fuel-coolant mixing for the second explosion. In one test in saturated water, multiple trigger sites were observed but no propagating explosion resulted. Two distinct, but additive, energy conversion ratios were calculated from the test results. Based on pressure records and debris velocities, a kinetic energy conversion ratio, η_{KE}, had calculated values between 0.3 and 1.6 percent. A conversion ratio, η_p, related to the work done in pressurizing the chamber air ranged between 0.2 percent and 8.6 percent. The total fraction of the melt thermal energy converted, $\eta_{tot} = \eta_{KE} + \eta_p$, reached a value of 9.9 percent in an experiment involving a double explosion, but in this case, the value of η_{KE} was limited to 1.3 percent.

14 DOCUMENT ANALYSIS — a KEYWORDS/DESCRIPTORS	15 AVAILABILITY STATEMENT
	NTIS GPO Sales
	16 SECURITY CLASSIFICATION (This page)
b IDENTIFIERS/OPEN ENDED TERMS	Unclassified (This report) Unclassified
	17 NUMBER OF PAGES 86
	18 PRICE